

This is a repository copy of Reaction kinetics of Na2CO3-activated blast furnace slag with organic ligands: insights from electrical conductivity measurements.

White Rose Research Online URL for this paper: https://eprints.whiterose.ac.uk/id/eprint/232925/

Version: Published Version

Article:

Tchio, J.A. orcid.org/0000-0001-6347-608X, Adesanya, E., Sliz, R. et al. (2 more authors) (2025) Reaction kinetics of Na2CO3-activated blast furnace slag with organic ligands: insights from electrical conductivity measurements. Cement and Concrete Composites, 160. 106021. ISSN: 0958-9465

https://doi.org/10.1016/j.cemconcomp.2025.106021

Reuse

This article is distributed under the terms of the Creative Commons Attribution (CC BY) licence. This licence allows you to distribute, remix, tweak, and build upon the work, even commercially, as long as you credit the authors for the original work. More information and the full terms of the licence here: https://creativecommons.org/licenses/

Takedown

If you consider content in White Rose Research Online to be in breach of UK law, please notify us by emailing eprints@whiterose.ac.uk including the URL of the record and the reason for the withdrawal request.



ELSEVIER

Contents lists available at ScienceDirect

Cement and Concrete Composites

journal homepage: www.elsevier.com/locate/cemconcomp





Reaction kinetics of Na₂CO₃-activated blast furnace slag with organic ligands: Insights from electrical conductivity measurements

Julson Aymard Tchio ^{a,*} , Elijah Adesanya ^a, Rafal Sliz ^c, Brant Walkley ^b , Juho Yliniemi ^{a,**}

- ^a University of Oulu, Fibre and Particle Engineering Research Unit, P.O. Box 8000, FI 90014, Finland
- ^b School of Chemical, Materials, and Biological Engineering, University of Sheffield, UK
- ^c Optoelectronics and Measurement Techniques Unit, University of Oulu, 90570, Oulu, Finland

ARTICLE INFO

Keywords: Electrical conductivity Pore solution Ligands Blast furnace slag Reaction kinetics

ABSTRACT

Electrical conductivity measurement using impedance spectroscopy could be a valuable technique for monitoring the various reaction processes of cementitious materials and predicting their long-term durability. In this study, alternating current impedance spectroscopy was employed to investigate the influence of two ligands, 2,3-dihydroxynaphthalene and 3,4-dihydroxybenzoic acid with a 0.1 wt% dosage, on the hardening process of four types of blast furnace slag (BFS) activated with sodium carbonate solution. The objectives of the study were to investigate whether impedance spectroscopy could be used for estimating the reactivity of BFS and monitoring the reaction kinetics of this type of binder as well as evaluating the correlation between electrical conductivity and reaction heat, pore solution chemistry, setting time, flowability and compressive strength. The results demonstrated that both ligands accelerated the hardening process and increased compressive strength, which was confirmed by the various techniques used. The measured electrical conductivities varied among BFS pastes due to differences in their pore solution composition and microstructure and correlated with compressive strength evolution. The results demonstrated that impedance spectroscopy is sensitive enough to detect differences in conductivity due to differences in the reactivity of BFS and the effect of low a dosage of ligands in the binder. However, because of the overall complexity of reactions in this type of binder, responses in electrical conductivity do not show systematic trends.

1. Introduction

In recent years, numerous climate change and global warming phenomena have been observed worldwide, with unprecedented temperature variations of up to 1.5° above the pre-industrial reference period [1]. One of the causes of climate change is carbon dioxide emissions from Portland cement production, which accounts for 8–10 % of global CO₂ emissions [2–4]. Close to 50 % of the carbon dioxide emissions generated by cement production originates from the calcination of limestone, while the remaining CO₂ emissions come from the combustion of fuels required to provide the thermal energy necessary for Portland cement production [5]. The development of sustainable binders as alternatives to traditional Portland cement is crucial for reducing the carbon footprint of the construction sector. Blast furnace slag (BFS), a by-product of the iron and steel industry, has proven to be a promising raw material to produce sustainable binders as

supplementary cementitious materials (SCM) or as precursor in alkali-activated binders. Alkali-activated BFS binders exhibit good physico-mechanical properties and improved durability compared to Portland cement [6,7]. However, the alkali activation process involves complex chemical reactions and mechanisms which influence the performance and the resulting microstructural formation of the binder.

Several BFS alkaline activators have been reported in the literature, such as sodium hydroxide (NaOH), sodium silicate, magnesium carbonate, sodium sulphate (Na₂SO₄) and sodium carbonate (Na₂CO₃) [2, 8]. One of the most sustainable alkali activators for BFS is sodium carbonate, as it has lower CO_2 emissions compared to other common activators like sodium silicate or sodium hydroxide and is cheaper [9]. Although the early-age properties of BFS binders activated with Na₂CO₃ solution are often low, at a later age, this activator impacts the development of the microstructure and physico-mechanical properties. Similarly, the reactivity of the BFS itself plays a crucial role in

E-mail addresses: julson.tchio@oulu.fi (J.A. Tchio), Juho.Yliniemi@oulu.fi (J. Yliniemi).

^{*} Corresponding author.

^{**} Corresponding author.

determining the properties of the obtained binders. Formation of reaction products (calcium silicate hydrate (C-S-H), calcium aluminium silicate hydrate (C-A-S-H), monosulfoaluminate, stratlingite, hydrotalcite, gismondine, etc.) when BFS is activated depends on the chemical composition of the material. Furthermore, the chemical composition of different types of BFS has an impact on reactivity and consequently strongly influences phase formation [2,3,10,11]. The effect is either due to the dissolution rate of the glass or the type and structure of the hydrates formed, although it also depends on the activating solution and consequent pore solution composition. Sodium silicate activation studied by Dai et al., [12] produced rapid silicate polymerization and a distinctive C-A-S-H gel structure, while a hydroxide activation solution demonstrated a faster initial reaction but different phases assemblage evolution. In the case of Na₂CO₃, the formation of gaylussite, and calcium bearing phase (calcite) are critical early age products and there is a correlation between carbonate concentration and reaction kinetics [13]. Lui et al. [14] revealed how carbonate ions influence the calcium silicate hydrate gel and nanostructure.

Cement admixtures are increasingly being used in cementitious materials due to their impact on controlling the hardening process, providing improved workability and higher compressive strength [15]. Among the most used cement admixtures are superplasticisers, retarders and accelerators, as these modify the properties of mortar, cement paste and concrete. Luukkonen et al. [16] showed that lignosulfonate-based superplasticisers provided better workability for alkali-activated blast furnace cement compared to other superplasticisers commonly used in Portland cement. They attributed this behaviour to the different pH levels in the two systems. Organic ligands such as 2,3-dihydroxynaphthalene (2,3-DHN) and 3,4-dihydroxybenzoic acid (3,4-DHBA) have been studied as potential admixtures for BFS binders. They have the ability to complex ions (Ca, Al, Mg, Fe), which reduces the concentration of free ions in the solution, leading to a system to promote further BFS dissolution which can potentially accelerate the early-age solidification process [7,15]. This aligns with the work of Xu et al. [17] who explored the impact of various alkanolamines on the hydration process of Portland cement and found that alkanolamine can significantly alter dissolution, product formation and the microstructure evolution. The microstructural pore connectivity investigation by Chi et al., [18] have provided some crucial information in pore network connectivity development with the aids of Ligands and its relationship to strength development. Nevertheless, the reaction process of BFS with organic ligands is not yet well understood and requires the use of new characterisation techniques beyond commonly used methods such as SEM coupled with EDX testing, setting time, isothermal calorimetry and XRD

Alternating current impedance spectroscopy (ACIS) is an electrochemical technique that has been used to study the reaction process of Portland cement-based materials. It allows for understanding the physical and chemical changes that occur in the binder's microstructure during hydration and solidification [20,17]. This method reveals different mesostructures and material properties, enabling the observation of variations in ion concentration in the pore solutions and the progressive formation of cementitious materials from water or an alkaline solution over time [21]. These changes result in a modification of the material's resistivity/conductivity, allowing for rapid and effective testing and responses. For instance, Lie et al. [22] and Otergar et al. [23] demonstrated that by incorporating SCMs into cement, particularly on the hardened mortar, this technique could assess the SCM impact on the material's electrical resistivity. Similar observations were made by Bortoletto et al. [24] when studying paste and hardened alkali-activated binders. Sosa Gallardo et al. [20] showed that electrical resistivity could be used to monitor the reaction process of Portland cement at an early stage. Using the same method, Torrents et al. [25] studied the electrical resistivity of ion migration in the pore solution with the addition of a superplasticizer and its effect on the setting time. They found that a superplasticiser extends the dormant period and increases the electrical conductivity, leading to a delay in setting time. Gu et al. showed that the high-frequency resistance of cement paste is primarily determined by its porosity and the ion concentration in the pore solution [26]. While ACIS has been applied to Portland cement systems, the pore solution chemistry and reaction pathway of Na₂CO₃-activated BFS binders is different from that of Portland cement hydration, which is likely to result in distinct ACIS responses. Thus it would be useful to study different binders systems using ACIS in detail. Additionally, it is unclear whether ACIS can effectively distinguish the reactivity of different BFS sources and the influence of organic ligand admixtures on the electrical conductivity and early-age hardening of these binders. Although calorimetry provides insights into reaction kinetics through heat flow measurements, electrical conductivity may offers a complementary approach by tracking ion migration processes and microstructural evolution, particularly during later stages when solid-liquid phase modifications and progressive porosification of the activated slag facilitate continued ion transport aspects that cannot be fully captured by calorimetric techniques alone. Therefore, the objectives of this study are to investigate the applicability of alternating current impedance spectroscopy (ACIS) for studying the reaction process and reactivity of different blast furnace slags, and the influence of organic ligand admixtures on the early-age properties of sustainable Na₂CO₃-activated blast furnace slag binders.

2. Materials and methods

2.1. Raw materials and sample preparation

Four different types of BFS were sourced from four different countries for use in this study: France (BFS-FR), Finland (BFS-FI), Japan (BFS-JP) and England (BFS-EN). The chemical composition of the slags is shown in Table 1. The selection of BFS samples was based on their variation in chemical composition, as well as factors such as the raw materials used and the production processes that differ from one steel mill to another, which consequently can lead to different reactivity of BFS. The particle size distributions (PSD) of different BFS were determined using a Beckman Coulter LS 13320 and the results are illustrated in Fig. 1.The D₁₀, D₅₀ D₉₀ of each BFS differ from each other (BFS-FR (D $_{10}\,{=}\,1.21~\mu\text{m},$ D $_{50}\,{=}\,9.61~\mu\text{m},$ D $_{90}\,{=}\,27.20~\mu\text{m})$ BFS-FI (D $_{10}\,{=}\,1.45~\mu\text{m},$ $D_{50} = 11.58~\mu\text{m},\, D_{90} = 30.11~\mu\text{m}),\, \text{BFS-JP}\,\, (D_{10} = 1.20~\mu\text{m},\, D_{50} = 9.14$ $\mu m,~D_{90}=29.14~\mu m)$ BFS-EN ($D_{10}=1.20~\mu m,~D_{50}=8.91~\mu m,~D_{90}=8.91~\mu m$ 26.41 μm)). Sodium carbonate (Sigma-Aldrich, Belgium) was used as the alkaline activator. This was used to prepare a solution with a concentration of 2 mol/l. The ligands used were 2,3-dihydroxynaphthalene (Sigma-Aldrich, Belgium) and 3,4-dihydroxybenzoic (Tokyo Chemical Industry, Co Japan).

2.2. Sample preparation

The BFS samples were prepared at room temperature (20 ± 3 °C); they were activated by using a 2 mol/L Na₂CO₃ solution prepared by dissolving anhydrous Na₂CO₃ (212 g) in deionized water (1L) with a final solution pH of 11.77 and a conductivity of 10.2 S/m. The activating solution was mixed with BFS at a solution-to-slag mass ratio of 0.4. A dosage of 0.1 wt% of the mass of BFS of 2,3-dihydroxy naphthalene (2,3-DHN) and 3,4-dihydroxybenzoic (3,4-DHBA) was incorporated into the BFS based on an earlier study [7] to observe the influence on BFS dissolution. In this study the BFS samples with no ligand are referred to as BFS-Fr-N, BFS-Fi-N, BFS-Jp-N, BFS-EN-N. The samples with a ligand are called BFS-Fr-2,3-DHN, BFS-Fi-2,3-DHN, BFS-Jp-2,3-DHN, BFS-EN-2,3-DHN, BFS-Fr-3,4-DHBA, BFS-Fi-3,4-DHBA, BFS-Fr-3,4-DHBA, BFS-EN-3,4-DHBA, BFS-EN-3,4-DHBA, BFS-EN-3,4-DHBA, BFS-EN-3,4-DHBA, BFS-EN-3,4-DHBA, BFS-EN-3,4-DHBA, BFS-EN-3,4-DHBA, BFS-EN-3,4-DHBA, BFS-EN-3,4-DHBA for the 3,4-dihydroxybenzoic ligand.

Table 2 shows the proportions of the precursors of the samples prepared. A total mass of 450 g of BFS was weighed, into which sodium carbonate solution containing 0.1 % ligand was added. A mixer was then

Table 1Chemical composition of different BFS.

Oxides (%)	CaO	Al_2O_3	${ m SiO}_2$	MgO	Fe_2O_3	Cl	SO_3	Na ₂ O	${ m TiO_2}$	K ₂ O	MnO_2
BFS-FI	36.5	13.2	34.1	12.3	0.5	0.09	1.9	0.5	2.05	0.76	0.33
BFS-FR	40.2	12.1	34.2	7.05	0.5	0.04	0.8	0.2	0.8	0.42	0.21
BFS-EN	42.2	9.4	37.3	6.2	0.4	0.0	0.7	0.1	0.4	0.32	0.28
BFS-JP	43.4	13.1	33.5	5.2	0.4	0.04	0.6	0.18	0.5	0.3	0.16

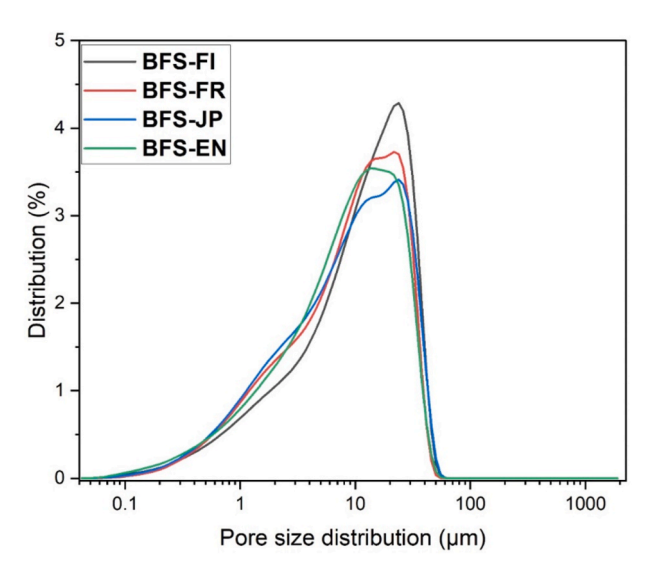


Fig. 1. Particle size of different BFS.

 Table 2

 Mix design of different BFS paste samples (g: grams).

	BFS- FI [g]	BFS- FR [g]	BFS- JP [g]	BFS- EN [g]	Na ₂ CO ₃ - 2 mol/L [g]	2,3- DHN [g]	3,4- DHBA [g]
BFS-FR-	450	-	-	-	180	-	-
N							
BFS-FR-	450	-	-	-	180	0.45	-
2,3-							
DHN							
BFS-FR-	450	-	-	-	180	-	0.45
3,4-							
DHBA							
BFS-FI-	-	450	-	-	180	-	-
N							
BFS-FI-	-	450	-	-	180	0.45	-
2,3-							
DHN							
BFS-FI-	-	450		-	180	-	0.45
3,4-							
DHBA							
BFS-JP-	-		450	-	180	-	-
N							
BFS-JP-	-	-	450	-	180	0.45	-
2,3-							
DHN							
BFS-Ja-	-	-	450	-	180	-	0.45
3,4-							
DHBA							
BFS-EN-	-	-	-	450	180	-	_
N							
BFS-EN-	-	-	-	450	180	0.45	-
2,3-							
DHN							
BFS-EN-	-	-		450	180	-	0.45
3,4-							
DHBA							

used to combine the different components for 3 min to form a

homogeneous cement paste. An amount of 230 g of the cement paste was transferred into a custom-designed cell, as described in Fig. 2, for impedance spectroscopy measurement, the curing of the samples was done at ambient temperature. Prior to initiating the impedance spectroscopy analysis, the cell containing the sample was subjected to 2 min of vibration to minimise the presence of air bubbles. For strength determination, samples were cast into plastic moulds (2 cm \times 2 cm), covered with a plastic bag, cured and demoulded after 24 h (hr). After demoulding, the samples were cured in an ambient environment (with a relative humidity of 70 % and a temperature of 21 \pm 3 °C) until the age of the mechanical tests (1, 3, 7, 14 and 28 days).

2.3. Characterisation methods

2.3.1. Setting time and compressive strength

Initial and final setting times, according to EN 196-3, were determined by applying 86 penetrations during the first 15 h after mixing, using Vicatronic apparatus (Matest, E044N). To determine the flowability, the paste sample was evaluated using a flow table test, following the standard procedure described in Ref. [27]. The average of the two diameters was reported as the spread diameter.

The compressive strength tests were carried out using a calibrated Zwick/Roell (Z100) machine with a maximum load of 100 kN and a loading capacity at a constant displacement rate of 1.8 mm/min. Four different samples were used and the average strength was reported.

2.3.2. Isothermal microcalorimetry

Isothermal calorimetry tests were conducted to analyse the hydration of the mixes in the first 3 days after mixing according to the ASTM C1679 standard procedures (ASTM International, 2017), using an 8-channel TAM Air isothermal calorimeter (TA Instruments) at 23 $^{\circ}\text{C}$. A plastic ampoule holder was used for the samples and deionized water was used as a reference. The samples were first prepared by mixing for 3 min at 800–1000 rpm and then transferred to the plastic ampoule, which was then loaded into the calorimeter. The reported results were normalised by the total mass of the fresh paste of each sample. The first 45 min of hydration captured by the calorimeter was not used as sample mixing was done ex-situ.

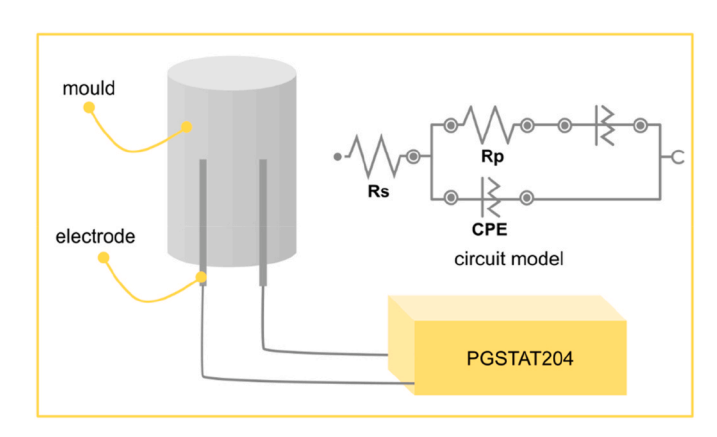


Fig. 2. Custom cell and circuit model.

2.3.3. Element concentration analyses

Inductively coupled plasma mass spectrometry (ICP-MS) was used to determine the pore solution composition extracted from the pastes. The pore solution was extracted at early ages (1 h, 6 h and 24 h of reaction) using an Instron 3000 universal testing machine. A titanium cylinder with an inner diameter of 6.5 cm, outer diameter of 16 cm and height of 28 cm was used. The pore solution was extracted with a loading of 400 MPa at a rate of 1 kN/s. The pore solution squeezed by a high-pressure system was collected by a vessel with nitrogen as the protective gas to avoid carbonation. Then, ICP-MS was employed to determine the concentration of Ca, Na, K, Mg, Al, Fe, Si and S.

2.3.4. Impedance spectroscopy

Impedance spectroscopy measurements were carried out using a single channel impedance analyser (Metrohm AutoLab, PGSTAT204) connected to a custom cell with two electrodes (stainless steel electrodes). The custom cell was designed using a cylindrical plastic container with dimensions of 6×12.2 cm; the dimensions of this mould and the position of the electrodes (length, width) were chosen based on the work and results carried out by Sosa Gallardo in 2021 and 2022 (Fig. 2) [20,17]. ACIS measurements were carried out at room temperature over a frequency range from 1 MHz to 100 Hz, with an applied disturbance amplitude of 10 mV and a current range of up to 1 mA. The frequency range of 1 MHz-100 Hz, as indicated by prior research on Portland cement impedance spectroscopy, demonstrated significant responses in impedance analysis. This included the response of the bulk cement paste and the interfacial response between the cement matrix and the electrode. To obtain sufficient information at an early age, the AC impedance measurement was done at 5 min, 30 min, 1 h, 6 h and 24 h, then at 3 days, 7 days, 14 days and 28 days. Before data acquisition, two control experiments were conducted to account for variability caused by the measurement system and cabling. Each sample was measured three times to improve the power of the statistical data and minimise random error. During the measurement, the samples were sealed with plastic due to the sensitivity of the sample's resistivity to moisture content and temperature, which affects the certainty and relevance of the analysis.

The overall resistance was obtained from the measurement of AC impedance, according to the equivalent circuit model $R_s((RpCPE)CPE)$ illustrated in Fig. 2. The choice of this model was made based on its high accuracy in simulating the responses of cement paste from alternating current. In this study, the overall resistance is considered as the sum of the resistance of the liquid and the solid R_s and the liquid-solid interface

resistance R_P [28,29]. The different circuit parameters were determined using Nova software from Autolab after fitting. Rs and R_P represent the total resistance of the solid and liquid phases, and CPE represents the constant phase element of the paste. The index t illustrates the variation of resistance over time. It should be noted that in impedance spectroscopy the Na_2CO_3 -activated BFS is considered as a circuit model, and the bulk resistance is determined at high frequency, which allows determination of the overall resistance. Also, the possible variation of temperature during hardening in different samples may influence the measured conductivity in this model. Conductivity measurements were obtained from the resistivity of each cementitious paste by dividing the global paste resistance by the cell constant, which was obtained by measuring different concentrations of Na_2CO_3 solution at low concentrations (0.01, 0.1 and 1 mol Mol/L), as described in the literature [30].

3. Results and discussion

3.1. Results

3.1.1. Influence of ligand on setting time and flowability of Na₂CO₃-activated BFS

The ligands influenced the setting time of the Na₂CO₃-activated BFS, as shown in Fig. 3. The initial and final setting times were reached at varying times when incorporating 2,3-DHN and 3,4-DHBA although an exception was observed for BFS-EN, which took a longer time to set. This indicates that 2,3-DHN and 3,4-DHBA act as setting time accelerators in the Na₂CO₃-activated BFS system. However, the mechanism and the extent of their influence appear to vary depending on the specific reactivity or chemical composition of the BFS. Previous research [7,14] has demonstrated that organic ligands (2,3-DHN and 3,4-DHBA) enhance BFS dissolution through their complexing capabilities and it appears that this increase in dissolution coincides with the acceleration of setting time. This suggests that the ligands that complex dissolved ions temporarily enhance dissolution, but also precipitation reactions leading shorter setting times. Both ligands improved the flowability of the pastes compared to the references and 3,4-DHBA improved it more than 2,3-DHN, as shown in Fig. 3b. This trend was consistent across all the BFS pastes used.

3.1.2. Compressive strength

The strength of the samples increased with curing age with and without ligands, as illustrated in Fig. 4. Incorporation of the ligand increased the compressive strengths in the early and late stages. 2,3-

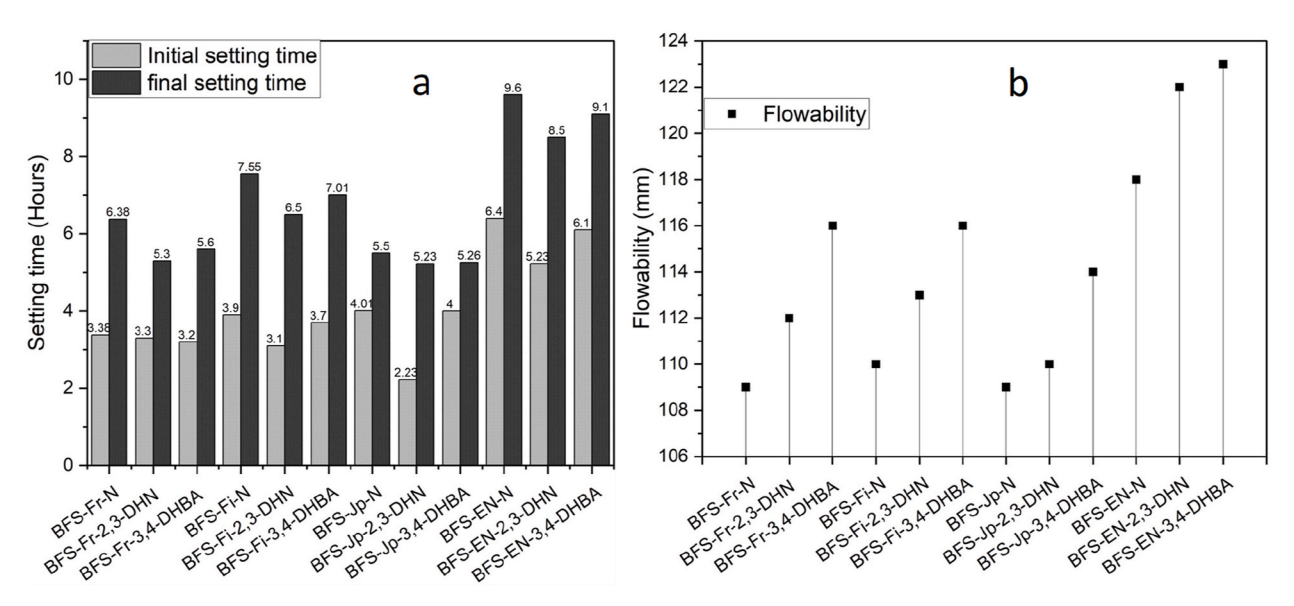


Fig. 3. Setting time and flowability.

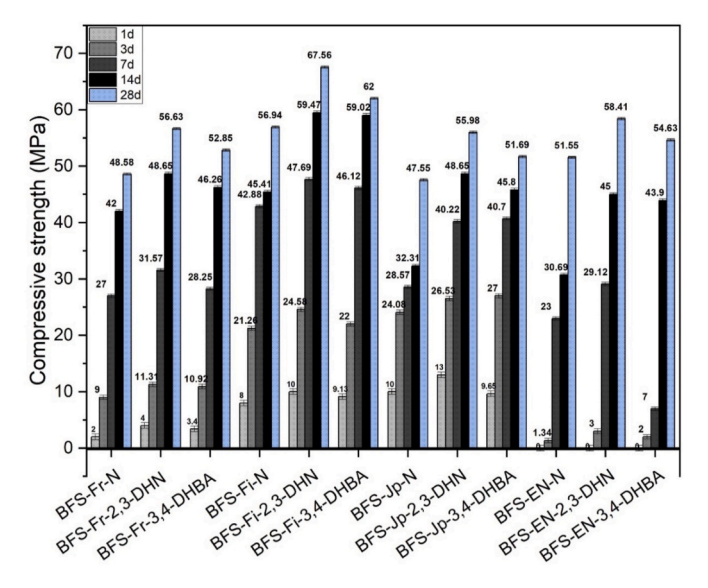


Fig. 4. Compressive strength of the pastes.

DHN had a greater effect on the strength development of Na_2CO_3 -activated BFS than 3,4-DHBA. The changes in the strength development of the different samples suggest that the ligand impacted the hardening process of the BFS. The early-age strength of the BFS-EN paste (1, 3 and 7

days) was very low compared to the other BFS samples even when incorporating ligands, showing its lower reactivity compared to other BFS samples. Thereafter, at 28 days BFS-EN with both ligands showed higher compressive strength than the reference sample. Additionally, the BFS-Fi samples (BFS-Fi-N, BFS-Fi-2,3-DHN, BFS-Fi-3,4-DHBA) showed higher compressive strength than the others, which could be attributed to the higher MgO content which can have an influence on strength development [3]. According to Ben Haha et al. [3], high MgO content (>5 %) in BFS results in the formation of strength-contributing hydrotalcite-like phases. In the BFS-Fi samples, the MgO content (See Table 1) was 12.3 % in comparison with 6.2 % in BFS-EN. The effect of 2.3-DHN on strength development corroborates the work carried out by Ramaswamy et al. [7]. Evidently, the compressive strength of Na₂CO₃-activated BFS is not governed solely by the MgO content. This observation reflects the influence of the aluminium content on compressive strength, as the 13.1 wt% aluminum content in BFS-Jp resulted in greater strength than the 9.4 wt% in BFS-EN. This suggests that high Al₂O₃ and MgO content is more conducive to reactivity. This interpretation corroborates the work of Matthes et al., [31] who demonstrated that the reactivity of BFS increases with the content of CaO and Al₂O₃ whereas it decrease with SiO₂, FeO, and TiO₂. However, there is no linear relationship between oxide content and material reactivity over a wide composition range [27,28,32].

3.1.3. Reaction kinetics

The calorimetric curves of the BFS samples with and without ligands during the first 80 h after mixing are illustrated in Fig. 5. The reaction

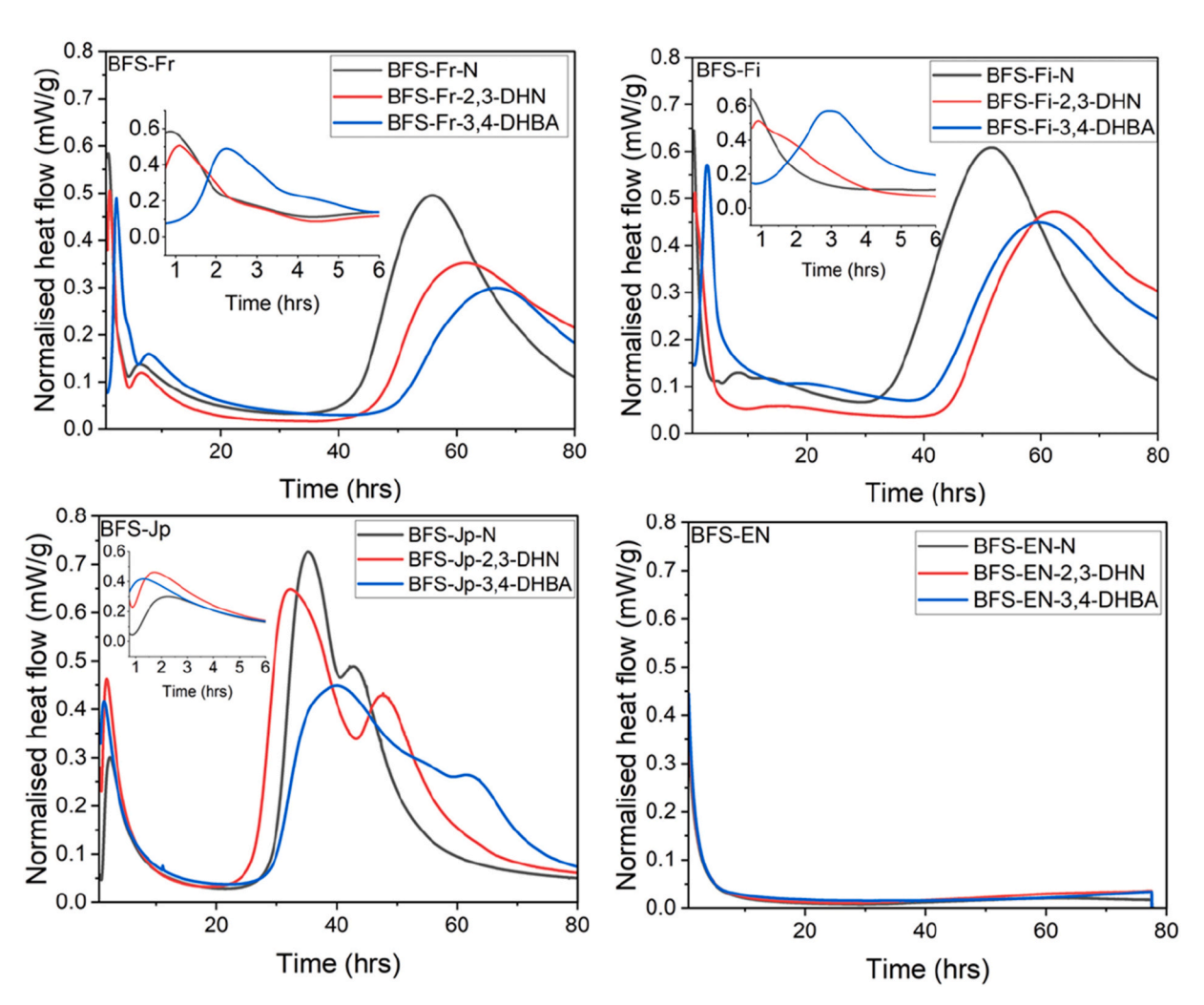


Fig. 5. Normalised heat flow of different blast furnace slags determined via calorimetry.

peaks detected through calorimetric measurements signify a stage characterised by significant chemical reactivity. As ligands are incorporated into the BFS, they prolong the induction period and shift and widen the peaks of the main exothermic peaks during 20-80 h. This change in the intensity of the peak indicates that the functional groups of the ligand affect the reaction kinetics. For BFS-Fr and BFS-Fi, both ligands delayed the main heat flow peak compared to the reference (BFS-Fr-N, BFS-Fi-N), although for BFS-Fr the reaction was prolonged, especially with 3,4-DHBA. For BFS-Fi, both ligands show similar patterns, but the peaks are higher with 2,3-DHN. On the other hand, for BFS-Jp the ligands cause an earlier rise in the main heat flow peak and BFS-Jp-2,3-DHN shows a sharper, more intense peak, while BFS-Jp-3,4-DHBA shows a broader, less intense reaction. Of the two ligands, 2,3-DHN accelerated the reaction kinetics of BFS-Fr, and BFS-Fi based on the first exothermic peaks and 3.4-DHBA accelerated the reaction kinetics of BFS-Jp, based on the intensity of the first exothermic peaks.

The setting time in Fig. 3a aligns well with the calorimetry observations. The samples with no ligands in BFS-Fr, BFS-Fi and BFS-Jp that show high heat flow peaks generally exhibit longer setting times, while those with lower intensity peaks that contain ligands show shorter setting times. In contrast with the other samples, BFS-EN correlates with the extended setting times, suggesting slower reaction kinetics. For BFS-EN no major exothermic picks were observed during the first 80 h, reflecting the slow reactivity and delay in the formation of reaction products at early stages, which is in line with the compressive strength results.

The total reaction heat released shows the difference in the heat

evolved in the presence of and without ligands (Fig. 6), indicating the difference in reaction kinetics among different BFS samples due to the presence of ligands. The BFS-EN heat release was significantly lower than that of other BFS, which correlates with the observed lower strength at an early age. It has been noted that there is not necessarily a direct correlation between the heat of reaction and mechanical strength development, but the main hardening reactions typically start somewhere along the reaction peak after the final setting time in a Portland cement system [33], which may be different in the Na₂CO₃ system. Nonetheless, this reactivity does not directly correlate with mechanical strength, as it can also be affected by variables such as microstructural evolution, pore structure development and the characteristics of the reacted product [2,25]. The variation in heat flow observed between the calorimetry curves suggests that reactive oxides (CaO, MgO, Al₂O₃, SiO₂ etc.) differ in their content or accessibility, resulting in unique hydration behaviour when interacting with the ligands. The basicity of slag samples was evaluated using two distinct ratio calculations. The CaO/SiO₂ ratio demonstrated significant variation among samples: BFS-Fi (1.07), BFS-Fr (1.17), BFS-EN (1.13), and BFS-Jp (1.29). A more comprehensive assessment utilizing the (CaO + MgO)/(SiO2+Al₂O₃) ratio, which incorporates the contributions of magnesium oxide and alumina, vielded values of 1.031, 1.02, 1.036, and 1.04 for BFS-Fi, BFS-Fr, BFS-EN, and BFS-Jp, respectively. While BFS-Jp exhibited the highest basicity in both calculations, suggesting enhanced hydraulic reactivity potential and correlating with its observed higher heat flow during the initial 3 days of reaction, the relationship betweenthe basicity ratios and performance characteristics showns an unexpected pattern. This deviation from the

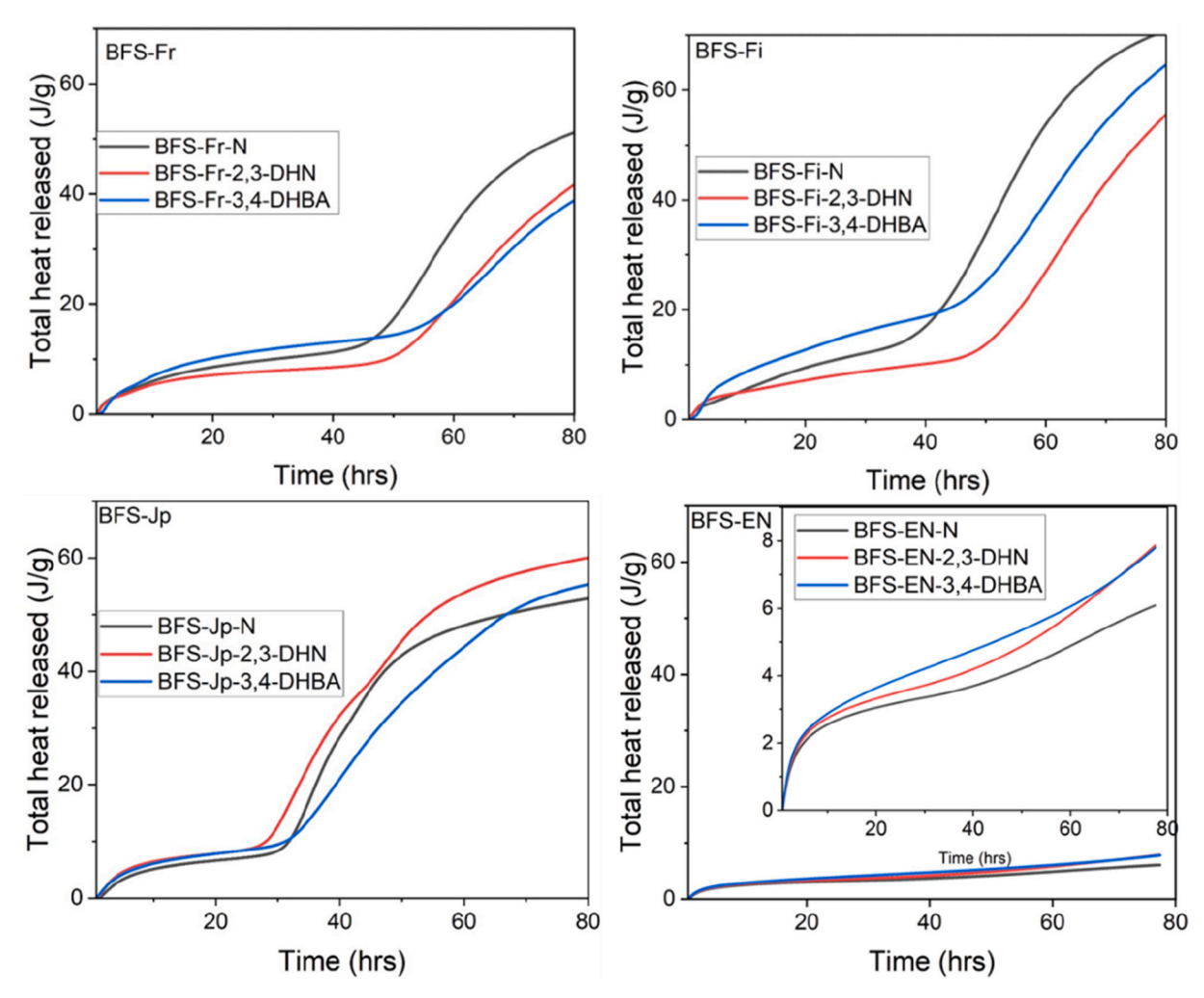


Fig. 6. Total heat released of different blast furnace slags determined via calorimetry.

established literature data indicates that high basicity values do not necessarily translate into enhanced reactivity or superior mechanical strength in these slag systems [34,35].

3.1.4. Analysis of pore solution over time

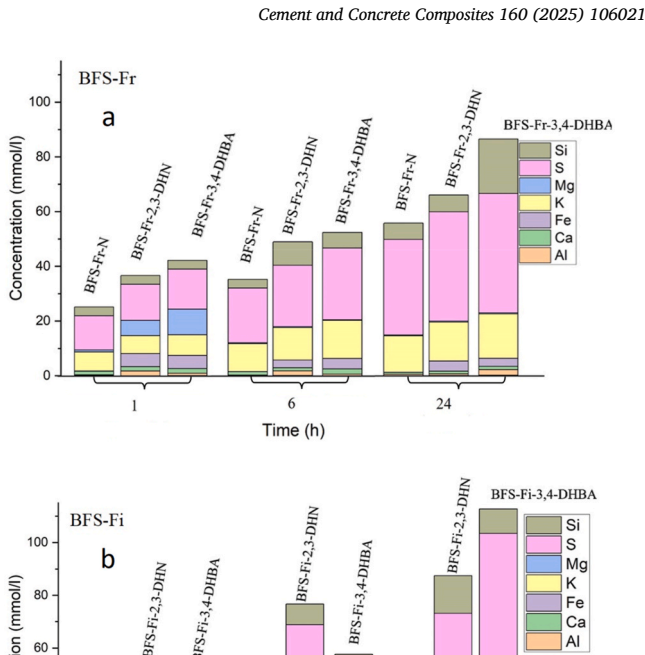
The concentration changes in the ions extracted from pastes over the first 24 h are shown in Fig. 7. The y-axis scale for BFS-FR, BFS-FI and BFS-JP differs from that of BFS-EN due to its higher ion concentration in mmol/l. In all samples without ligands, the total concentration of ions (Al, Ca, Fe, K, Mg, S and Si) is lower compared to samples with ligands, showing that ligands increase the concentration of ions in the pore solution. These ion concentrations vary during the first 24 h.

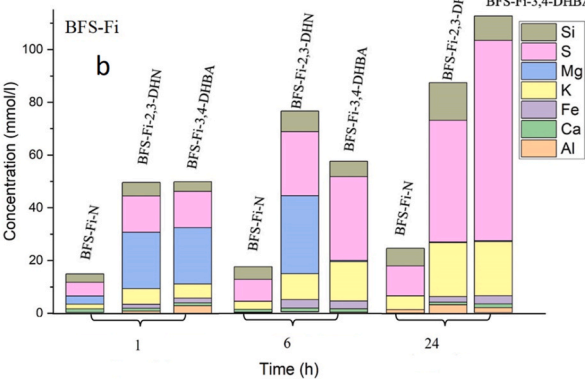
The case of BFS-FR, BFS-FI, BFS-JP and BFS-EN, the ion concentration trends are similar but with varying in proportions. Si is one of the main elements involved in the formation of cementitious phases and thus of high relevance. Si concentration varies according to the type of BFS. However, in general, the Si concentration increased slightly with time and decreased after 24 h, indicating the precipitation of phases. except in two systems: BFS-Fr-3,4DHBA and BFS-Fi-2,3-DHN, in which an increased Si was observed.

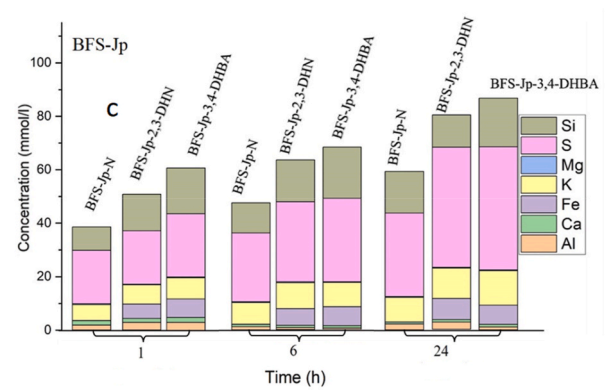
The highest concentration was detected for S despite it being present in low quantities in the BFS samples (Table 1). This shows its highly soluble nature and its limited ability to participate in the formation of phases in this type of binder system within the first 24 h. Interestingly, the S concentration in the BFS-Jp pastes was the highest, despite having the lowest SO3 content, as determined by XRF. Mg is expected to precipitate as Mg(OH)2 or other Mg phases when the pH is above 10.6, evidenced by its absence in most samples. However, ligands were able to increase the Mg concentration at 1 h and 6 h in BFS-Fi and BFS-Fr, which also had the highest MgO content of the studied slags. The ability of 3,4-DHBA and 2,3-DHN to increase the Mg concentration in batch dissolution experiments at pH 12 and in pore solutions in a similar binder system has been reported in earlier studies [7,15]. At later hours, the Mg concentration dropped, indicating that Mg participates in phase precipitation and that the ligands lost their ability to solubilise Mg.

Calcium, was present in minor concentrations and only in three of the studied systems: BFS-FR, BFS-FI and BFS-JP. In BFS-Fr, during the 1, 6 and 24 h periods, the proportion of Ca ions remained relatively stable with a slight increase when the ligands were incorporated; this stability could indicate a balance between the dissolving Ca and its consumption in the precipitation reactions. Also, it indicates that ligands interact more with other ions than with Ca, which is in line with earlier studies [7,15].

The concentration of Al remained low for all samples and times, with the exception of BFS-EN, in which a high Al concentration was detected already at 1 h, followed by a considerable increase at 6 h, and finally a significant decrease at 24 h. This behaviour demonstrates the rapid dissolution of Al followed by precipitation after 24 h. It would be expected that Al phases such as C-A-S-H or ettringite (due to high S concentration) could precipitate, but apparently that did not occur as the Al and S concentration remained high. This raises the question of whether it could be that Ca is the limiting element that prevents the formation of cementitious phases at early stages and explains the low strength development for the BFS-EN sample. This would be unexpected since Ca should be one of the most soluble elements in these experimental conditions. In other BFS samples, there is a fluctuation in the Al concentration over time when ligands were incorporated. The slight coherence between BFS-Fr and BFS-Fi for Al contrasts with their different behaviour for other ions, highlighting the complex interactions at play in this type of binder. The trend of Al concentration in BFS-Jp was similar to that of Ca where a decrease in concentration was noted between 1 h and 6 h, followed by a slight increase at 24 h. This similarity suggests possible coupled reactions involving both Ca and Al ions in the formation of products such as C-A-S-H or hydrotalcite. This observation is supported by Lothenbach et al. [11] and also correlates with the strength results presented in Fig. 4.







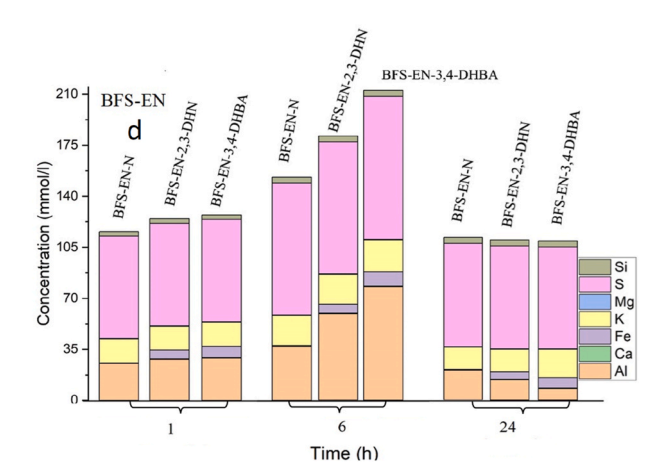


Fig. 7. Pore solution composition of different BFS. 7a: BFS-Fr, 7b: BFS-Fi, 7c: BFS-Jp, 7d: BFS-EN.

One of the most remarkable observations concerned the presence of Fe in the pore solutions. Despite the low iron oxide content (between 0.6 wt% and 0.4 wt%) in all BFS samples, Fe was detected in the pore solution when ligands were incorporated, suggesting that ligands have the ability to solubilise Fe by forming complexes, as supported by earlier studies [7,15]. This solubilisation is more significant in BFS-Jp than in BFS-Fr, BFS-Fi and BFS-EN. While Fe-containing cementitious phases are rare in BFS-based binders due to low Fe content, it is possible that Fe could participate in the formation of certain phases. For example, according to thermodynamic modelling, a low concentration of Fe could lead to the formation of mackinawite (FeS) [36].

Due to the use of Na₂CO₃ as the activating solution, the

concentration of Na in the pore solution significantly exceeded that of other ions. Graphs illustrating Na concentrations have been included in the Appendix. Na concentrations showed consistent trends in the BFS-Fi and BFS-EN samples, characterised by an increase in Na concentration between 1 h and 6 h, followed by a decrease at 24 h. Conversely, BFS-Jp and BFS-Fr samples exhibited a progressive decrease in Na concentration from 1 to 24 h. The reduction in Na concentration typically indicates the formation of phases such as C-(N,A)-S-H or N-(C-)A-S-H, although in the case of Na₂CO₃-activated BFS the formation of metastable gaylussite (Na₂Ca(CO₃)₂•5H₂O) is also likely. This suggests that, in the BFS-Jp and BFS-Fr samples, the formation of these phases may be accelerated and predominant compared to the BFS-Fi and BFS-EN

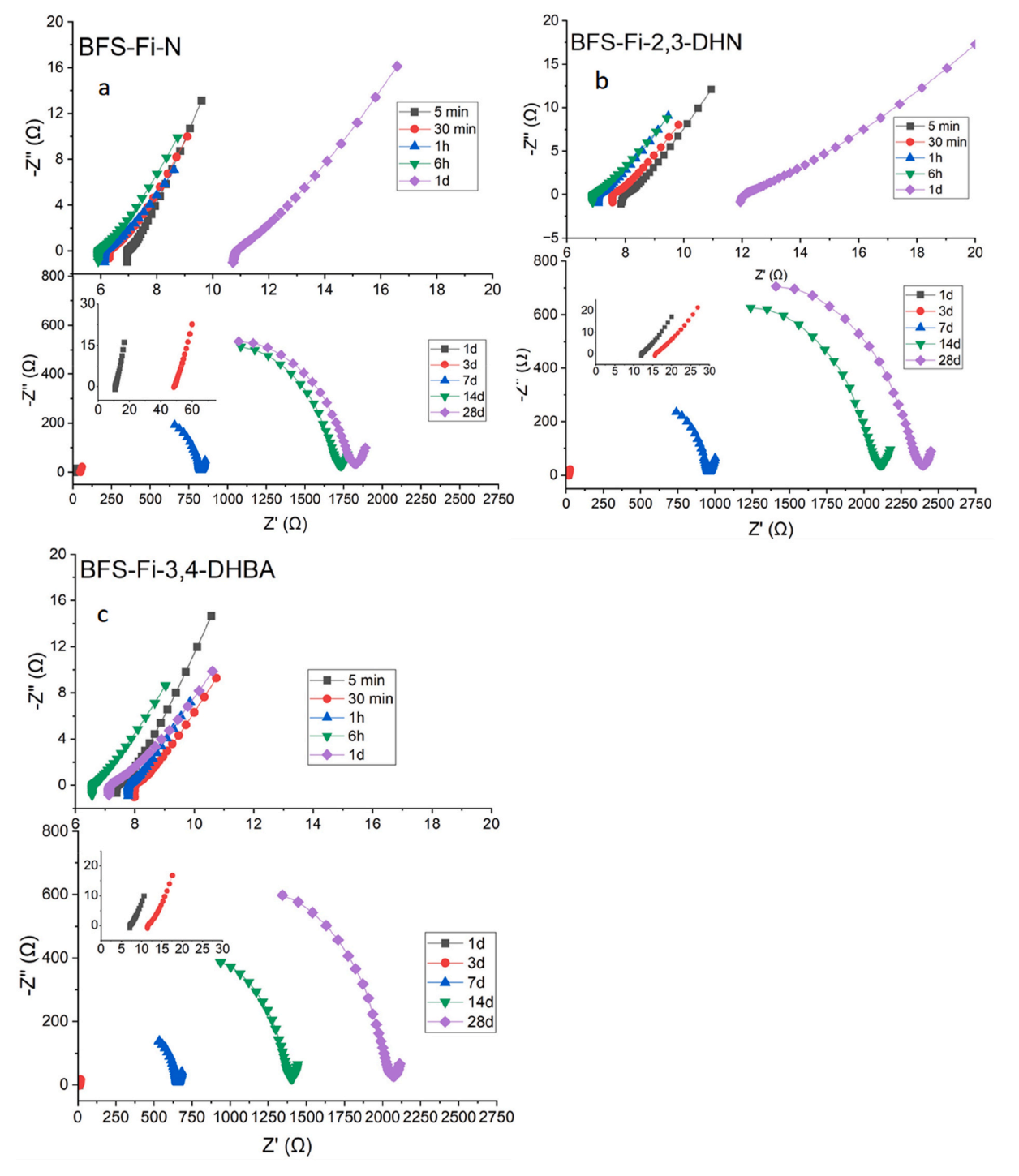


Fig. 8. Nyquist plot of BFS-Fi with and without ligands (a: BFS-Fi-N, b: BFS-Fi-2.3-DHN, c: BFS-Fi-3.4-DHBA).

samples. For BFS-Fi, a consistently lower Na concentration was measured (approximately 1000 mmol/L) compared to other slag systems (>3000 mmol/L), although the reason for this remained unclear. Rapid formation of Na-containing phases such as gaylussite or N-A-S-H could have occurred, but since the setting time and 1-day strength did not differ drastically from other samples, this explanation could not be the explaination.

3.1.5. Impedance spectroscopy and electrical conductivity

3.1.5.1. Impedance spectroscopy. Before proceeding with the interpretation of the results, it is important to note that using impedance spectroscopy for the investigation of cementitious binders involves four important factors: the solid particles of the cement paste, the electrolytic pore solution, the interface between the solid particles of the paste and the electrolyte solution, and the overall microstructure of the paste. These factors are crucial steps for alternating current to circulate within cement-based materials. By fitting the obtained impedance data to an equivalent circuit model, the parameters of the different circuit elements were determined using Nova 2.1 software, thus allowing the determination of the bulk electrical resistance of the BFS paste at early and later stages. Nova has specified the methodology for determining these circuit parameters [37].

An example of the impedance spectrum obtained for BFS-Fi with and without ligands is illustrated in Fig. 8 as a Nyquist plot to show the influence of the ligand on the evolution of the ohmic resistance of the BFS paste. The Nyquist plots for the other BFS samples have been added to Appendix. A change was observed in the ohmic resistance of BFS-Fi when the two types of ligands were used. This suggests that the interaction of the ligand affects the mobility and concentration of ions present in the pore solution during the dissolution process.

3.1.5.2. Electrical conductivity. Fig. 9 illustrates the electrical conductivity of BFS-Fi paste measured on a series of three identical, but separately prepared, samples. The objective of this experiment was to determine the margin of error associated with the same formulation during the first 24 h. It was found that the error in electrical conductivity was of the order of $0.015~\mathrm{S/m}$.

The electrical conductivity results for different BFS with or without ligands at different ages are presented in Fig. 10. According to these results, some chemical and physical changes occur during the dissolution, transport, nucleation stages and consolidation process of Na_2CO_3 -activated BFS. Initially, conductivity is mainly due to the BFS paste- Na_2CO_3 solution, which is close to 1–1.25 S/m. A rapid increase in

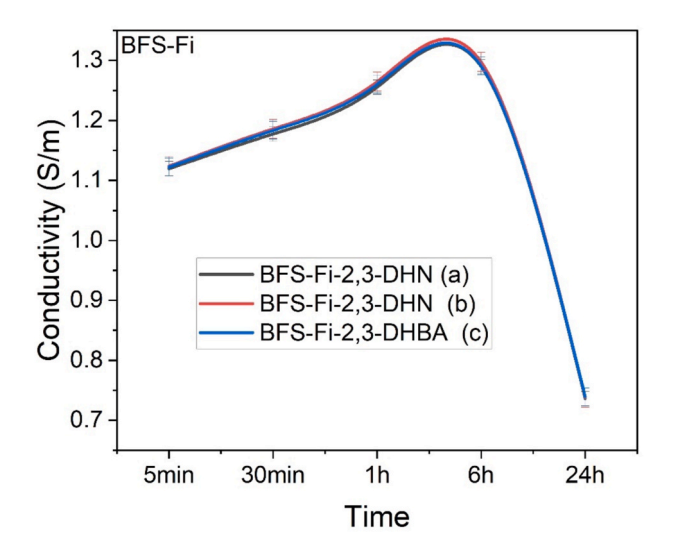


Fig. 9. Verification of the accuracy of the electrical conductivity measurement.

electrical conductivity can be observed for the BFS-Fr, BFS-Fi and BFS-Jp samples. This increase is termed the dissolution stage, where ions such as S, Ca, K, Mg, Al and Si from the slag dissolve with the aid of sodium carbonate solution to form the electrolytic solution. In contrast, for BFS-EN, a progressive decrease in electrical conductivity can be observed in the first hours, which is surprising considering that this sample had the highest concentrations of ions (Fig. 7). A high concentration of ions would be expected to provide higher electrical conductivity, but this was not the case, showing that the determined electrical conductivity is influenced by other factors aside from the concentration of ions in the electrolytic solution. For all BFS samples, the addition of the 2,3-DHN ligand led to a decrease in electrical conductivity compared to 3,4-DHBA and the reference samples during the first hour.

Depending on the BFS, a decrease in electrical conductivity was noted between 6 h and 24 h in the BFS-Fr, BFS-Fi and BFS-Jp pastes and an increase in the case of BFS-EN. The formation of cementitious phases leads to a considerable decrease in pore volume present in the matrix, thus inhibiting ion mobility. Consequently, ions are no longer able to move freely in the matrix, resulting in notable decrease in electrical conductivity. However, when ligands are added (1 h, 6 h and 24 h), the electrical conductivity is lower in BFS-FR, BFS-FI and BFS-EN compared to cases without ligand. In the case of BFS-Jp, conductivity with the 2,3-DHN ligand exceeds that of the reference at 24 h. Increased electrical conductivity of BFS-EN-N and BFS-2,3-DHN was observed at 24 h. However, with the 3,4-DHBA ligand, conductivity increased between 24 h and 3 days.

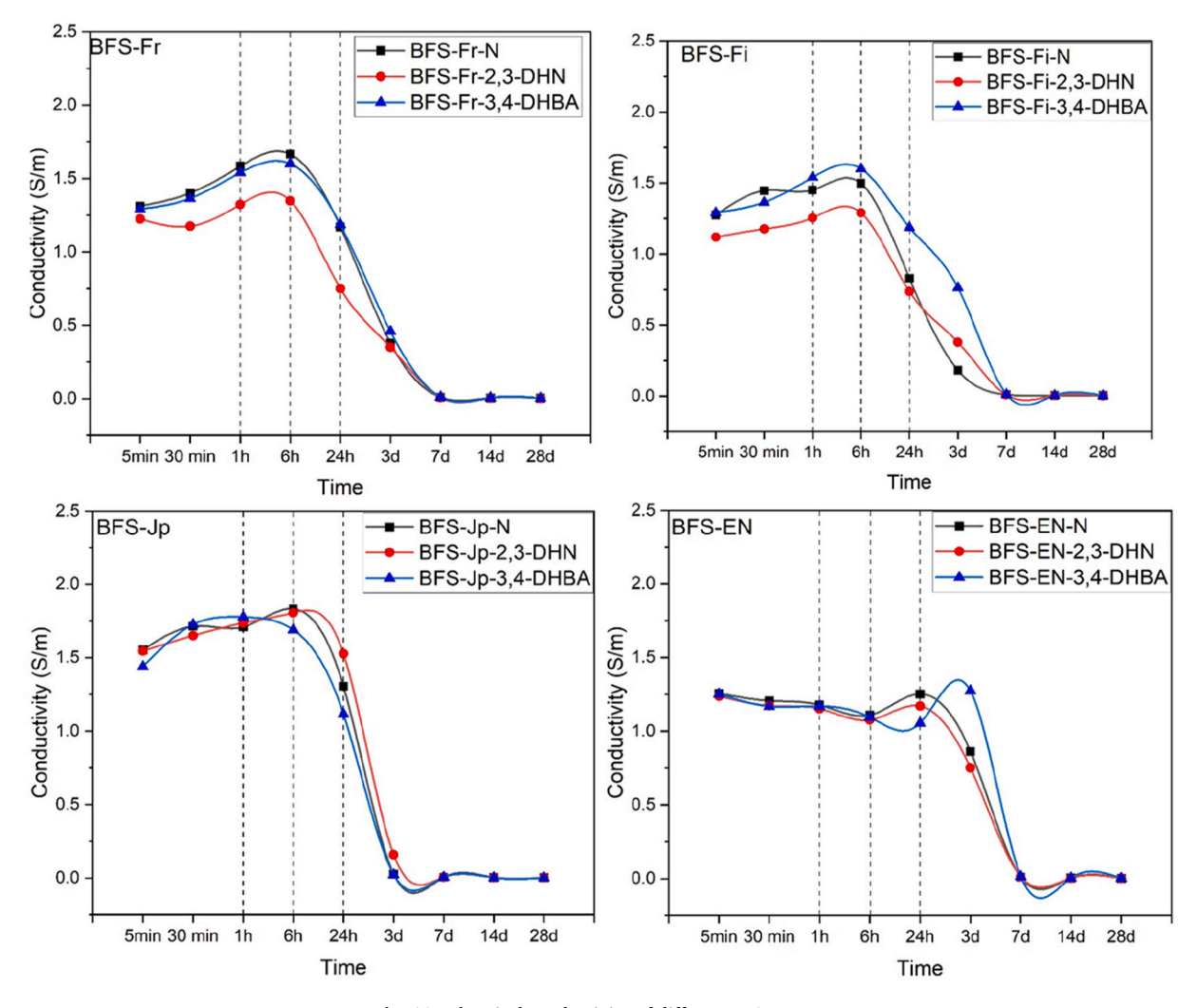
Between 1-7 days and 7–28 days, the formation of a stable and compact microstructure is responsible for the progressive decrease in electrical conductivity. By this stage, most ions present in the matrix have participated in phase formation.

3.1.6. Relationship between electrical conductivity and heat flow of Na₂CO₃-activated BFS

There have been attempts to establish the relationship between the electrical resistance, compressive strength and cumulative heat of Portland cement hydration [38–40]. Here, correlation (Pearson correlation coefficient) and regression analysis was performed using the experimental data. A correlation evaluation was done for heat flow and electrical conductivity (Fig. 11).

The normalised heat flow curve (solid line) and electrical conductivity (dotted line) of different BFS samples as a function of reaction time are illustrated in Fig. 11. During the dissolution and transport phases between 0 h and 6 h after BFS is mixed with the solution, the BFS mixtures show an initial heat flow peak corresponding to the dissolution stage. No exothermic peaks are observed in BFS-EN slags despite the higher ion concentration in the pore solution. When observing the different curves closely, it can be noted that electrical conductivity does not increasedirectly when the first heat peaks are observed. This evidently represents a physical change that cannot be detected by the heat of reaction, which may suggest an organisation of the matrix, a sort of sedimentation leading to progressive densification of the cementitious material that influences the ion mobility [41]. Variations in the electrical conductivity of all BFS samples may therefore reflect differences in densification and sedimentation in the microstructure, implying different connectivity between pores with and without ligands.

Between 6 h and 24 h, corresponding to the nucleation phase (induction period), the heat of reaction decreases to a minimum point, whereas conductivity is highest. Following this change in reaction heat, a progressive decrease in electrical conductivity at a slow rate is observed. This stage could mark the beginning of the precipitation of phases. The precipitation period indicates the consumption of conductive ions and densification of the matrix, leading to a reduction in pore connectivity in the microstructure, thereby reducing the transmission path of conductive ions in the pore solution, which further explains the progressive decrease in conductivity [20,17]. From 24 h to 72 h, the main exothermic peaks are observed on the heat flow curve, while



 $\textbf{Fig. 10.} \ \ \textbf{Electrical conductivity of different BFS pastes}.$

electrical conductivity continues to decrease. This suggests a continuation of the phase formation processes and changes in the pore structure of the BFS pastes.

3.2. Discussion

Analysis of the impedance spectroscopy data shows that the conductivity derived from the resistance of different $\rm Na_2CO_3$ -activated BFS pastes as a function of time highlights this characterisation technique as one of the methods that could be used to monitor the hardening process. The Nyquist plot curves (Fig. 8) show differences between samples with and without ligands at the level of ohmic resistance (z(ohm)), which can indicate the influence of ligands on the formation of microstructure and pore connectivity at early and later stages.

The combination of fresh and hardened state properties of pastes and heat flow, cumulative heat, pore solution composition and electrical conductivity has made it possible to reveal the effect of ligands in BFS pastes. As a general observation, the reaction kinetics, as evidenced by calorimetry data, show that early-stage conductivity does not necessarily correlate with enhancing early age (1–3 days) reactivity. For instance, BFS-Jp, with the aid of 2,3-DHN and 3,4-DHBA, exhibited higher conductivity in the first 24 h, leading to higher heat flow compared to BFS-Fi (second), BFS-Fr (third), and BFS-En (fourth). Their cumulative heat evolution and strength development at 3 days differ from one another. This apparent variation can be explained by considering that conductivity measurements primarily reflect ion mobility in

the pore solution and early age pore connectivity. In contrast, reaction progress depends on factors such as the rate of ion incorporation into the reaction product, the formation of solid phases, and their interphase characteristics, as well as changes in the pore structure.

The correlation between electrical conductivity measurements, reaction progression in Na₂CO₃-activated BFS systems and strength development exhibits a complex dependency on solid-liquid interfacial phenomena, particularly during different reaction stages. In early-stage reactions, the measured conductivity predominantly reflects bulk solution ionic mobility within the pore network continuity, necessitating normalisation by pore solution conductivity to accurately illustrate microstructural evolution independent of concentration effects. Additionally, conductivity is influenced by pore space connectivity and tortuosity, making comparison between mass transport properties and conductivity an interesting research topic for the future as it aligns with fundamental transport theory as conductivity and diffuse mass transfer share common dependence on pore network connectivity [42,43]. However, the post-setting period introduces significant complexity as the solid-liquid interface becomes the dominant factor in determining conductivity values through the formation of electrical double layers at the newly formed solid surfaces [44]. These interfacial phenomena fundamentally affect ion mobility and distribution patterns, where precipitated hydration products generate localized electric fields that significantly influence ion transport mechanisms and subsequent conductivity measurements. The pronounced decrease in conductivity post-setting, despite continued heat evolution, can be attributed to

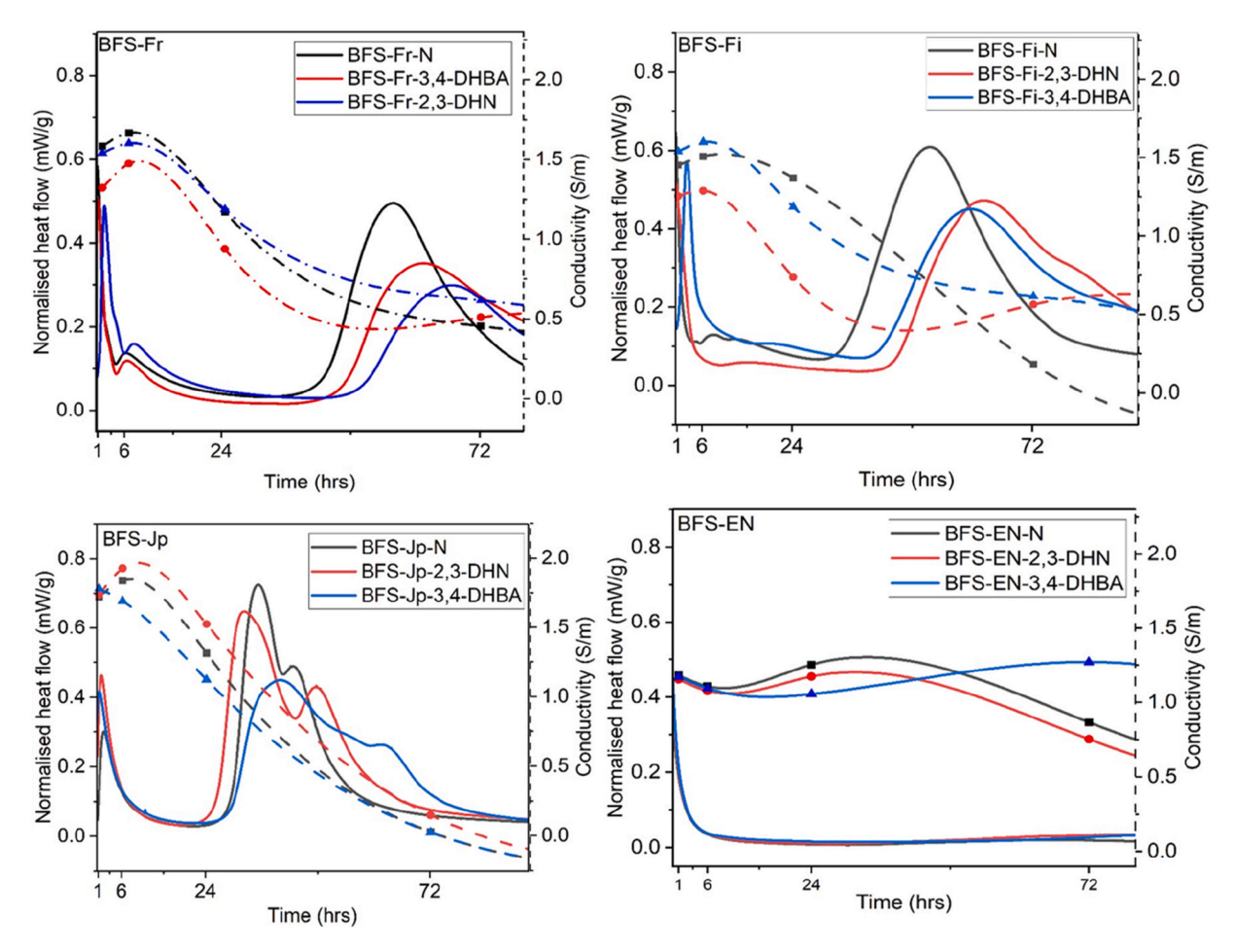


Fig. 11. Correlation between heat flow and electrical conductivity.

several interfacial mechanisms such as (i) the development of surface charges on precipitated phases, (ii) selective ion adsorption at solid-liquid interfaces, (iii) modified ion mobility within confined pore networks, and (iv) the formation of gel layers with distinct interfacial properties [42]. This complex interplay illustrates the non-linear relationship between conductivity and heat flow measurements throughout the reaction period. While calorimetric measurements reflect ongoing chemical reactions, conductivity measurements increasingly represent the sophisticated interaction between pore solution chemistry and evolving solid-liquid interfaces, necessitating careful interpretation when evaluating $\rm Na_2CO_3$ -activated BFS reactivity through conductivity measurements. It is also noted that these observations about the relationship between time-variant conductivity and BFS hardening reactions may differ significantly when other activators such as NaOH and sodium silicate are used.

The impact of ligands on the pore solution compositions of different BFS pastes measured during the first 24 h support earlier reports that the functional groups of ligands 2,3-DHN (-OH) and 3,4-DHBA (-OH, -COOH) have the capacity to complex ions such as Ca, Mg, Al and Fe [7, 15], which will increase the concentration of said ions in the pore solution. However, the pore solution compositions did not correlate with conductivity, which was an unexpected finding. BFS-EN had the highest concentration of ions in the pore solution but the lowest conductivity during the first 6 h reflecting the complex correlation between ion content and charge transport in Na₂CO₃-activated BFS systems. The pore solution analysis shows increasing free ion content, but electrical conductivity measurements demonstrate that the total ion content does not directly correlate with charge transport capability. This phenomenon can be attributed to the formation of ion pairs and complexes that reduce

ionic mobility, despite their presence in solution. Furthermore, the lower hydraulic reactivity of BFS-EN, evidenced by its delayed setting time and slower strength development, suggests that the dissolved ions may exist in less mobile forms or participate in preliminary reactions that reduce their contribution to conductivity. This is particularly relevant in systems where ion speciation and mobility, rather than absolute concentration, govern the measured conductivity. The relationship between ion concentration and conductivity is further complicated by changes in pore solution chemistry and the evolving microstructure during the early stages of reaction, where ions may be present but not effectively contributing to charge transport. This demonstrates that the overall electrical conductivity of these pastes is a combination of several factors. One such factor could be the effect of ligands acting as plasticisers, which can be seen in Fig. 3 as higher paste flowability. The plasticising effect leads to better dispersion of BFS particles, thus providing better workability [33,34]. This workability and dispersion improvement was more pronounced with 2,3-DHN than with 3,4-DHBA. Another factor could be the formation of complexes with different charges by the ligands in the pore solution [15]. Complexes with different sizes and charges have different conductivity, which could also influence the overall conductivity. This shows that ligands can have an effect via different mechanisms in the system, i.e. not only complexation of ions in the pore solution, but also interaction with the surface of BFS particles. The molecular structure of 3.4-DHBA consists of a benzene ring functionalised with two adjacent hydroxyl groups (-OH) at positions 3 and 4, and a carboxyl group (-COOH), establishing a tridentate binding site for metal complexation at pH 12-13. Thermodynamic modelling done by Bagheri et al., [20] reveals that the addition of 3, 4-DHBA lead to the formation of Fe(3,4-DHBA)₃⁻⁶ and Al(3,4-DHBA)₃⁻⁶

complexes with Fe and Al ions, respectively, while divalent cations (Ca, Mg) form $M^{2+}(3,4\text{-DHBA})_2^{-4}$ complexes. However, the chelating efficiency exhibits notable deterioration above pH 13, attributed to competitive hydroxide ion complexation [20]. Conversely, 2,3-DHN, characterized by a naphthalene ring system with vicinal hydroxyl groups at positions 2 and 3, demonstrates optimal functionality at pH 11.2, as illustrated by Ramaswamy et al., [7] facilitating enhanced ion dissolution kinetics and efficient complexation with Al, Fe, Si, Mg and Ca. The bidentate coordination site, formed by adjacent hydroxyl groups in conjunction with the extended $\pi\text{-system}$ of the naphthalene ring, promotes robust metal-ligand interactions under conditions where hydroxide competition is minimized.

The interaction of ligands with the surface of particles may create a repulsive force between particles. This is consistent with what has been found by Uchikawa et al. [41], who have shown that the repulsive force in cement paste varies according to the organic polymer admixtures used. For instance, in our study, the structural and electronic configurations of 2,3-DHN and 3,4-DHBA significantly influence their interaction mechanisms with Na₂CO₃-activated BFS systems and their complexing capability with ions, which is manifested in distinct performance characteristics. The enhanced compressive strength observed with 2,3-DHN can be attributed to its unique molecular architecture, through molecular-level interactions and their effects on particle dispersion and microstructure development [45]. The adjacent hydroxyl groups on the naphthalene ring generate substantial electrostatic repulsion through proximity-induced partial negative charges on oxygen atoms, coupled with significant steric strain [46] creating a more effective steric barrier around BFS particles during the early stages of reaction and facilitating the formation of connected pore that will favor reaction at a later stage. This could result in better initial particle dispersion, preventing premature agglomeration and allowing for more uniform dissolution of the slag particles. This electronic configuration potentially facilitates stronger interactions with metallic ions in the pore solution, leading to better particle agglomeration, and promotes the formation of more uniformly distributed pore networks during sedimentation. In contrast, 3,4-DHBA modified electronic and spatial properties, characterized by persistent hydroxyl group repulsion but modulated by carboxyl group-induced hydrogen bonding capabilities and reduced steric hindrance due to its smaller benzene ring, result in intermediate compressive strength development better than the reference samples, but less effective than 2,3-DHN. These molecular-level differences in electronic distribution and spatial arrangements fundamentally influence the ligands capacity to complex with dissolved species, thereby affecting the formation and development of strength-providing phases in the binder matrix through modified dissolution and precipitation kinetics. The observed differences in performance can be attributed to the balance between dispersive and aggregative forces during different stages of the reaction. The molecular structure of 2,3-DHN provides optimal dispersion during the critical early period, followed by controlled aggregation that promotes the formation of a more refined microstructure. This mechanism aligns with previous studies on organic modifiers in cementitious systems [41] where the molecular architecture plays a crucial role in determining the final material properties.

The experimental results demonstrate a difference between the reaction chemistry and mechanism of the Na₂CO₃-activated BFS system and cement system illustrated in the literature. In the Na₂CO₃-activated BFS system, the pore solution chemistry is initially dominate by Na and HCO₃ ions maintaining the pH values around 11.5 and 12.4 [7]. While in the Portland cement system, Ca and OH ions dominated the pore solution, which lead to a pH of more than 13. Additionally, the reaction of Na₂CO₃-activated BFS exhibits a distinctive feature such as the formation of sodium calcium carbonate (gaylussite and calcite) preceded by the development of C-A-S-H gel, which differs markedly from the one of Portland cement where C-S-H set-up directly [47]. The conductivity measurement generally starts to decrease from 2 h after mixing in a

Portland cement [42] which is the contrast in Na_2CO_3 -activated BFS where the conductivity increases during the first 6 h in BFS-Fr, BFS-Fi and BFS-Jp; depending also on the type of BFS the increase in conductivity may start at 6 h as observed in BFS-EN. It would be important to note that the HCO_3 ions in Na_2CO_3 solutions exhibit limited conductivity, as reported by Bernard et al. [48] due to their lower mobility resulting from weak electrolyte properties and incomplete dissociation in solution. Nevertheless, these ions maintain elevated pH levels, which is crucial for dissolution and precipitation during the BFS activation process. Additionally, despite their low mobility, HCO_3^- ions precipitate rapidly when mixed with BFS and participate in the formation of carbonate phase products [7].

The higher pore connectivity provided by the ligands would also favor reactions at later stages of hardening, allowing mechanical properties to evolve. The combination of electrical conductivity and heat flow thus highlights the fact that the dissolution of ions and their mobility between 1 h and 6 h can be detected by both impedance spectroscopy and isothermal calorimetry in Na_2CO_3 -activated BFS, as illustrated in Fig. 11. It is worth noting that no data points were collected between 24 h and 72 h due to the assumption that the densification of the BFS matrix over time would reduce pore connectivity, leading to a continuous decrease in electrical conductivity. This is because at this stage, reaction products are being formed, which releases exothermic heat easily detectable by calorimetry. However, the development of these reaction products leads to a modification of the microstructure, which in turn impacts the pore connectivity; the mobility of the ions is controlled by the state of the microstructure.

4. Conclusions

The main objectives of this study were to evaluate whether impedance spectroscopy could be used to evaluate the reactivity of Na_2CO_3 -activated blast furnace slags and to detect the effect of new types of admixtures (ligands). Based on the results, this characterisation technique can be used to study Na_2CO_3 -activated BFS, evaluate BFS reactivity and detect the influence of organic ligands, although the trends in electrical conductivity are not systematic and more research is needed to understand the underlying mechanisms. A comparison was made of impedance spectroscopy data on fresh and hardened properties of pastes, pore solution composition and reaction heat evolution was made. On this basis, the following conclusion can be drawn.

- The evolution of ohmic resistance allows monitoring of the hardening process, providing information on the dissolution process of BFS and microstructural development.
- \bullet High early-stage (<24 h) conductivity indicates high early-stage reactivity for Na₂CO₃-activated BFS pastes. However, the ligands that improved early-stage strength have lower early-stage conductivity compared to the reference samples.
- The effect of ligands on conductivity varies between BFS samples, and the differences in conductivity were not reflected systematically in compressive strength results.
- The use of 2,3-DHN and 3,4-DHBA ligands with 0.1 % dosage leads to an acceleration of precipitation reactions, thereby modifying the pore solution composition, density of the binder and consequently conductivity at later stages of the reaction.
- Ligands have varying effects on reaction kinetics and the fresh and hardening process, with different influences depending on the type of BFS used. The reactivity of BFS varies considerably depending on the chemical composition and the interactions of ligands on ions varies as well.
- The concentration of ions in the pore solution (first 24 h), even with
 the addition of a ligand, does not reflect the electrical conductivity of
 the different BFS pastes, possibly due to different interactions of the
 ligand on the surface of the BFS particles and complexation reactions
 in the pore solution.

CRediT authorship contribution statement

Julson Aymard Tchio: Writing – review & editing, Writing – original draft, Visualization, Validation, Methodology, Investigation, Formal analysis, Data curation. Elijah Adesanya: Writing – review & editing, Visualization, Supervision, Data curation. Rafal Sliz: Writing – review & editing, Validation, Methodology, Data curation. Brant Walkley: Writing – review & editing, Visualization, Supervision, Data curation. Juho Yliniemi: Writing – review & editing, Supervision, Resources, Project administration, Methodology, Funding acquisition, Data curation, Conceptualization.

Data availability

We have provided a link to access the research data [https://doi.org/10.23729/fd-f7b32f8f-8034-3efa-9f65-57e38c5ac064].

Declaration of competing interest

The authors declare that they have no known competing financial interests or personal relationships that could have appeared to influence the work reported in this paper.

Acknowledgements

This work was co-funded by the European Union under the Marie Skłodowska-Curie Action I4WORLD 101081280. However, the views and opinions expressed are those of the author(s) only and do not necessarily reflect those of the European Union or European Research Executive Agency [REA]. Neither the European Union nor the REA can be held responsible for them. JY acknowledges the Research Council of Finland (#354263). Additionally, the authors would like to thank the Centre of Material Analysis (University of Oulu) and the lab technicians (FPERU, University of Oulu) for their support with the material characterisation techniques.

Appendix

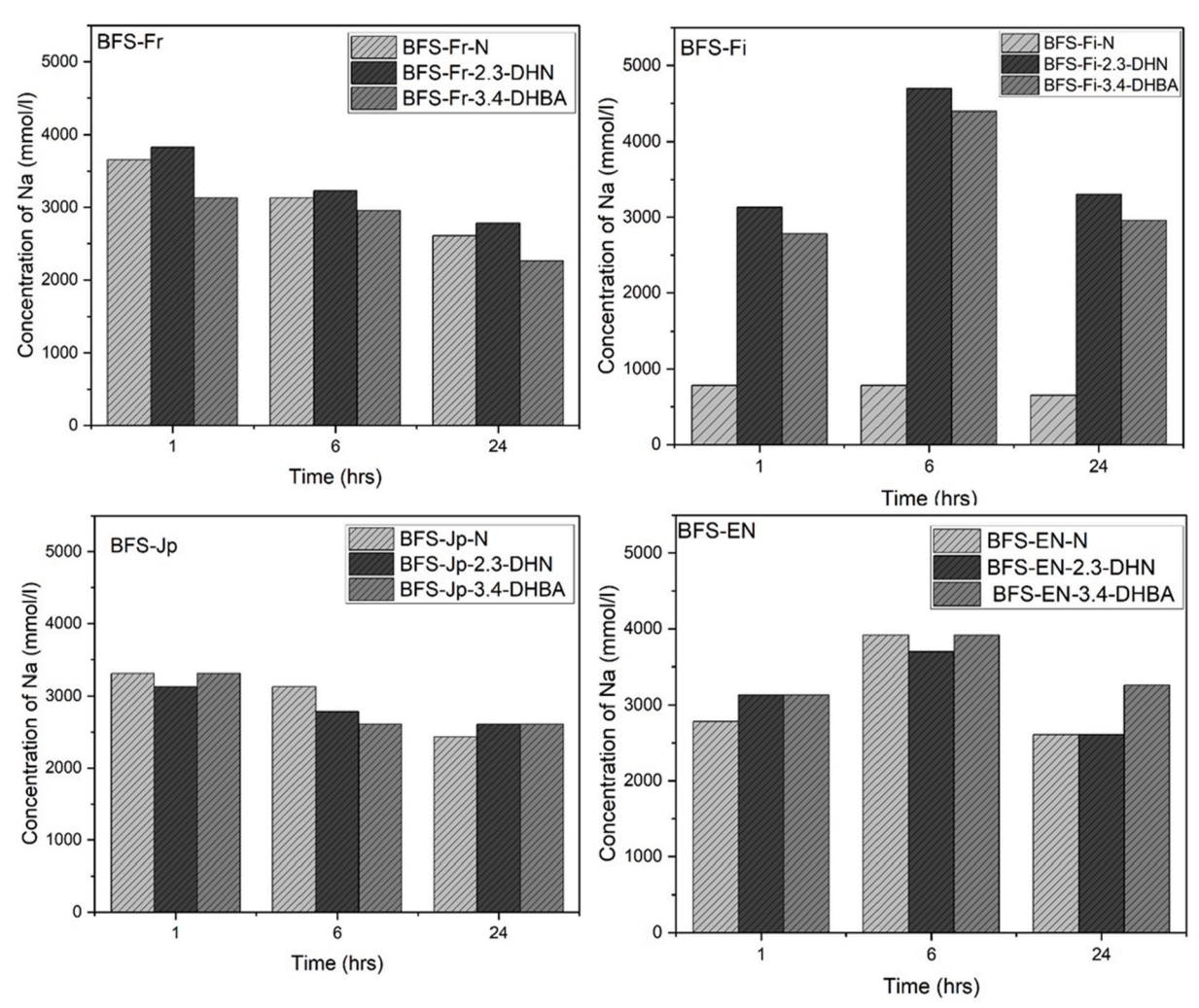
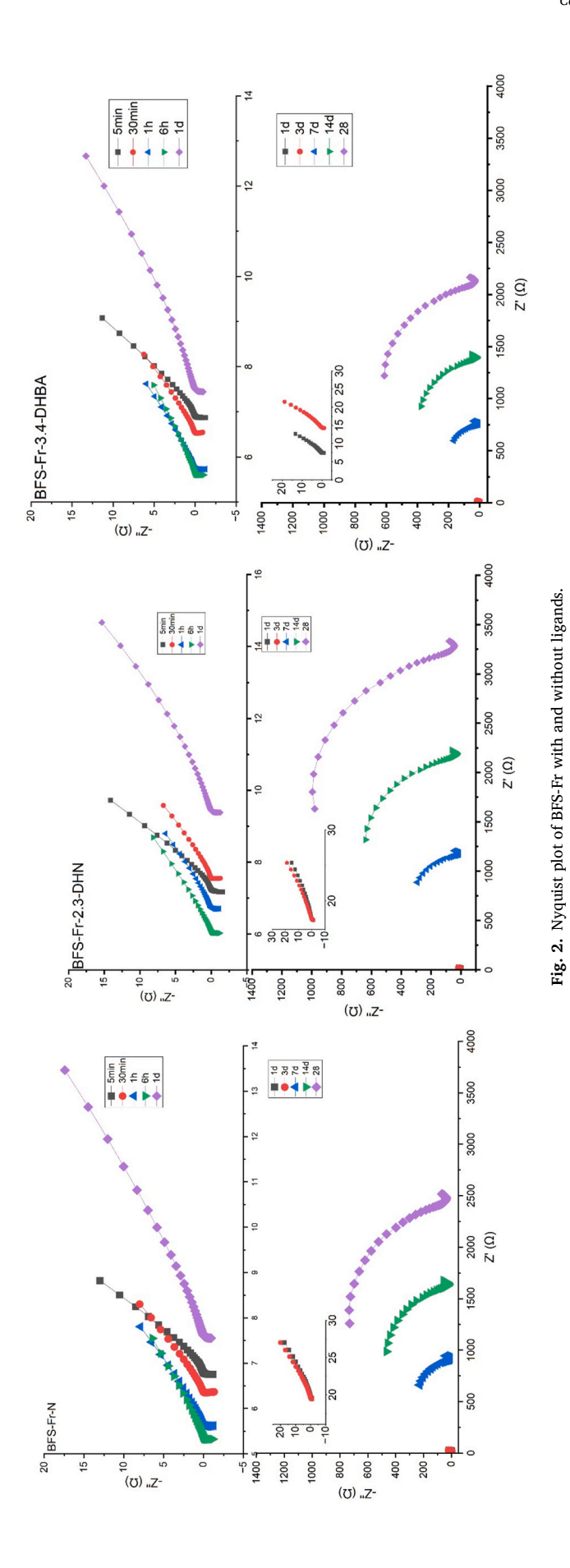
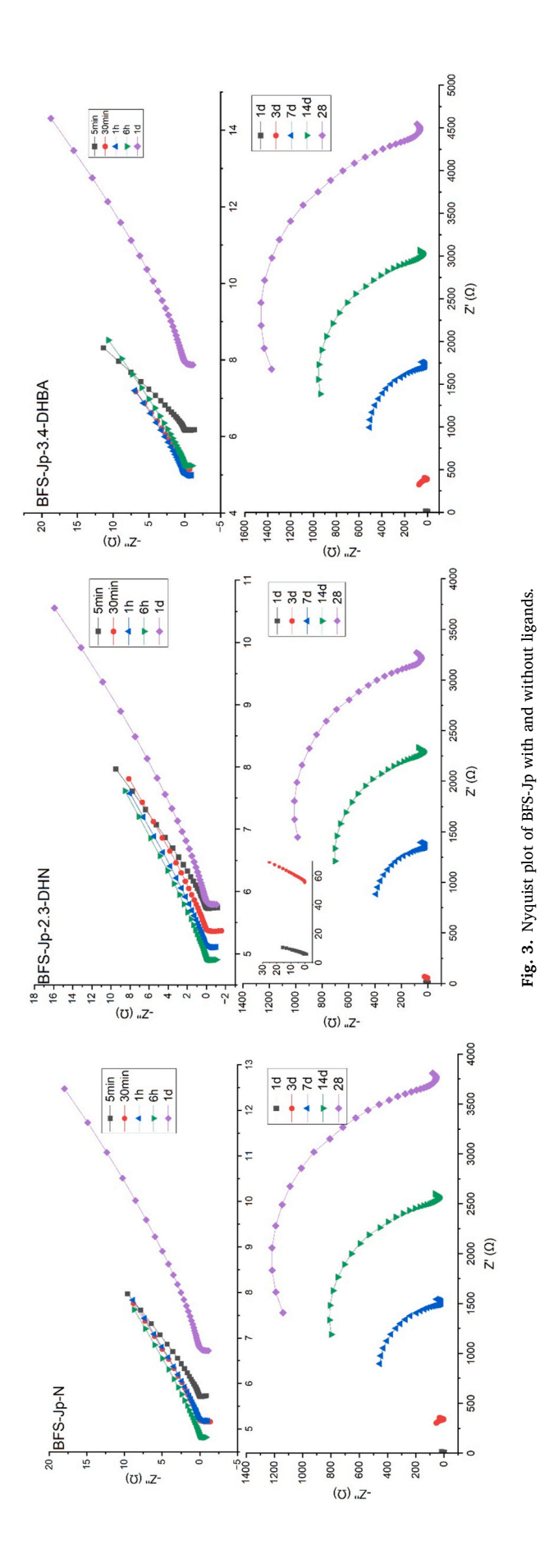


Fig. 1. Concentration of Na element in pore solution of different BFS.





15

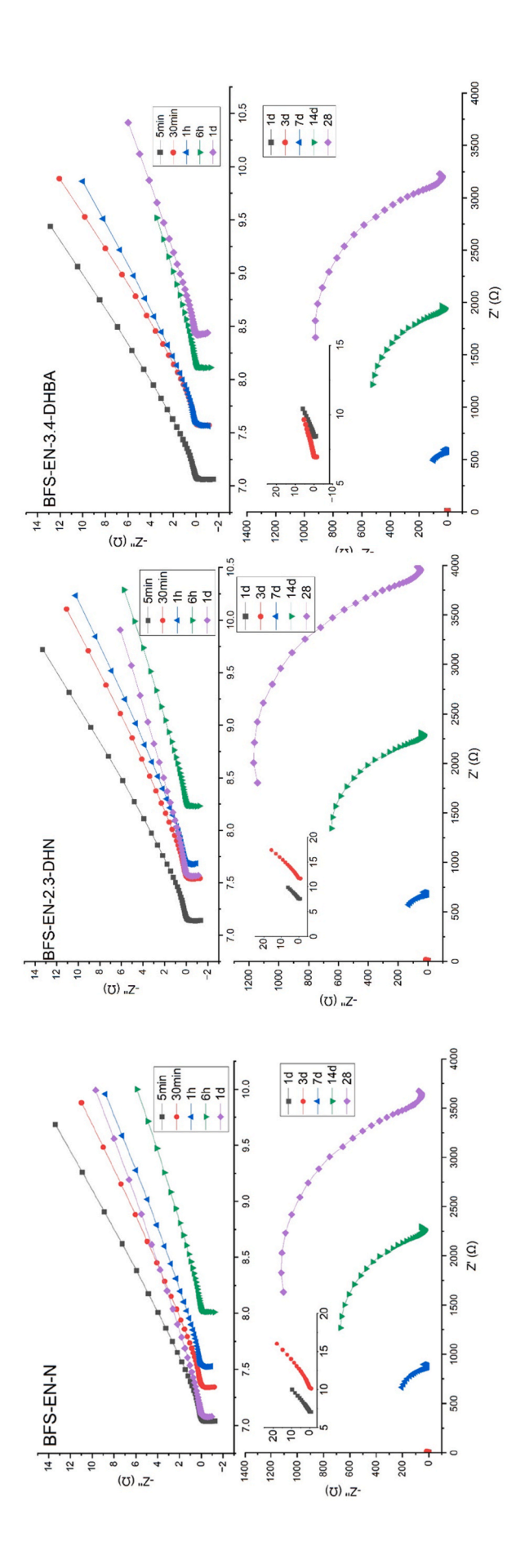


Fig. 4. Nyquist plot of BFS-EN with and without ligands.

16

Table 1Circuit elements parameter after fitting

	Fi-N					Fi-2.3DHN				Fi-3.4DHBA			
Time	Rs	Rp	CPE1	CPE2	Rs	Rp	CPE1	CPE2	Rs	Rp	CPE1	CPE2	
5min	5.949974	1	0.0003	9.00E-16	6.95	1	0.000564	9.00E-16	5.889991	1	0.000349	9.00E-16	
30 min	5.359975	1	0.001	9.00E-16	6.56	1	0.000751	9.00E-16	5.520041	1	0,0007014	9.00E-16	
1h	5.129984	1	0.001	9.00E-16	6.09	1	0.000675	9.00E-16	4.780028	1	0.00084	9.00E-16	
6h	4.899994	1	0.0006	9.00E-16	5.9	1	7.53E-04	9.00E-16	4.559979	1	0,0006954	9.00E-16	
1d	5.489993	1	0.0006	9.00E-16	11.09	1	7.44E-04	0.000312	6.499985	1	0,00097368	9.00E-16	
3d	47.691	1	0.0005	9.00E-16	15.763	7.6541	0.000187	0.00022	10.657	1	0,00055676	9.00E-16	
7d	204.38	620.9	2.79E-09	0.0003	236.5	717.24	2.32E-09	0.000326	194.87	460.83	4.68E-09	0.00039	
14d	264.87	1450	2.34E-09	0.0004	308.55	1777	2.43E-09	0.000378	254.03	1138.7	3.45E-09	0.000411	
28d	258.78	1548.2	3.39E-09	0.0002	334.06	2034.8	2.44E-09	0.00039	306.38	1744.4	2.17E-09	0.000595	
	Fr-N				Fr-2.3DHN	1			Fr-3.4DHBA				
Time	Rs	Rp	CPE1	CPE2	Rs	Rp	CPE1	CPE2	Rs	Rp	CPE1	CPE2	
5min	5.779967	1	0.000325	9.00E-16	6.2679	1	0.000275	9.00E-16	5.889991	1	0.000391	9.00E-16	
30 min	5.350033	1	0.000639	9.00E-16	6.5779	1	0.000947	9.00E-16	5.520041	1	0.000963	9.00E-16	
1h	4.619962	1	0.000706	9.00E-16	5.7307	1	0,0010597	9.00E-16	4.780028	1	0.001033	9.00E-16	
6h	4.340042	1	0.001038	9.00E-16	6.0708	0.53	1.59E-05	0.000709	4.559979	1	0.00155	9.00E-16	
1d	6.599956	1	0.000495	9.00E-16	9.4511	2.4015		0.000312	6.499985	1	0.00087	9.00E-16	
3d	19.598	3.89	0.000112	0,00016598	17.404	7.958	0.000145	0.000178	14.432	5.0069		0.000199	
7d	258.35	655.71	4.06E-09	0.000404	327.89	847.29	2.25E-09	0.000436	243.56	514.26	4.43E-09	0.000323	
14d	276.29	1352.2	4.07E-09	0.000457	361.37	1812.4	2.35E-09	0.000495	292.85	1095.4	3.86E-09	0.000388	
28d	266.79	2182.5	3.91E-09	0.000467	376.76	2876.3	2.46E-09	0.000469	313.76	1799.6	3.77E-09	0.000446	
	Jp-N				Jp-2.3DHI	N .			Jp-3.4DHBA	Α			
Time	Rs	Rp	CPE1	CPE2	Rs	Rp	CPE1	CPE2	Rs	Rp	CPE1	CPE2	
5min	4.7292	1	0.000549	9.00E-16	4.7568	1	0.000496	9.00E-16	5.185	1	0.000995	9.00E-16	
30 min	4.194	1	0.000717	9.00E-16	4.392	1	0.000707	9.00E-16	4.1576	1	0.000974	9.00E-16	
1h	4.2064	1	0.00072	9.00E-16	4.1273	1	0.000831	9.00E-16	4.0104	1	0.000931	9.00E-16	
6h	3.8568	1	1.46E-05	0.000664	3.9273	1	0.000795	9.00E-16	4.2682	1	0.000681	9.00E-16	
1d	5.822	1	0.000399	9.00E-16	4.8288	1	0.000502	9.00E-16	6.9738	1	0.000437	9.00E-16	
3d	160.37	177.9	3.23E-09	0.000389	53.036	3.02	0.000589	9.00E-16	164.61	222.87	4.71E-09	0.000545	
7d	242.04	1263.5	3.06E-09	0.000327	265	1091.8	2.81E-09	0.000344	250.43	1466.2	3.82E-09	0.000371	
14d	217.12	2326.6	2.91E-09	0.000373	269.58	2008.8	2.80E-09	0.00032	203.91	2795.4	2.88E-09	0.000396	
28d	186.42 EN-N	3540.9	0.000344	2.65E-09	265.19 EN-2.3DHN	2930.4	2.68E-09	0.000282	191.3 EN-3.4DHBA	4243.8	2.22E-09	0.000372	
Time	Rs	D-	CPE1	CPE2	Rs	D	CPE1	CPE2	Rs		CPE1	CPE2	
Time		Rp				Rp				Rp			
5min	6.0804	1	0.000326	9.00E-16	6.1904	1	0.000325	9.00E-16	6.079993	1	0.00032	9.00E-16	
30 min	6.377	1	0.000476	9.00E-16	6.5807	1	0.000456	9.00E-16	6.579962	1	0.000364	9.00E-16	
1h	6.5549	1	0.000622	9.00E-16	6.7232	1	0,00048712	9.00E-16	6.599956	1	0.000505	9.00E-16	
6h	7.027	1	0.001208	9.00E-16	7.266	1	0.001223	9.00E-16	7.129973	1	0.002413	9.00E-16	
1d	6.1057	1	0.000713	9.00E-16	6.5995	1	0.001267	9.00E-16	7.429999	1	0.001205	9.00E-16	
3d	9.316	1	0.000406	9.00E-16	10.828	1	0.000546	9.00E-16	6.000016	1	0.002022	9.00E-16	
7d	228.76	644.4	4.88E-09	0.000432	240.32	440.54	3.96E-09	0.000483	241.24	337.71	5.24E-09	0.000519	
14d	230.69	2002.1	3.62E-09	0.000772	332.83	1927.5	3.51E-09	0.000762	357.86	1566.7	4.05E-09	0.000821	
28d	171.07	3390.4	3.21E-09	0.000822	305.62	3602.2	3.79E-09	0.000599	330.7	2828.8	3.78E-09	0.000835	

Data availability

A link to the raw data is provided in the manuscript.

References

- L. Dahlman, Lindsey, "climate change: global temperature,", Clim. Chang. Glob. Temp. | NOAA Clim., 2024. https://www.climate.gov/news-features/unders tanding-climate/climate-change-global-temperature.
- [2] X. Sun, Y. Zhao, J. Qiu, J. Xing, Review: alkali-activated blast furnace slag for ecofriendly binders, J. Mater. Sci. 57 (3) (2022) 1599–1622, https://doi.org/10.1007/ s10853-021-06682-8.
- [3] M. Ben Haha, B. Lothenbach, G. Le Saout, F. Winnefeld, Influence of slag chemistry on the hydration of alkali-activated blast-furnace slag - Part I: effect of MgO, Cem. Concr. Res. 41 (9) (2011) 955–963, https://doi.org/10.1016/j. cempers 2011 05 002
- [4] J.A. Tchio, N. Yerima, C.R. Kaze, E. Kamseu, F.U. Chinje, C. Leonelli, Design and characterization of iron calcium aluminium silicate hydrate as low temperature binder, Innov. Infrastruct. Solut. 42 (1) (2024), https://doi.org/10.1007/s41062-023-01329-w. January.

- [5] V. Sousa, J.A. Bogas, Comparison of energy consumption and carbon emissions from clinker and recycled cement production, J. Clean. Prod. 306 (4) (2021), https://doi.org/10.1016/j.jclepro.2021.127277. April.
- [6] G.M. Kim, H.R. Khalid, H.J. Kim, H.K. Lee, Alkali activated slag pastes with surface-modified blast furnace slag, Cem. Concr. Compos. 76 (2017) 39–47, https://doi.org/10.1016/j.cemconcomp.2016.11.009.
- [7] R. Ramaswamy, M. Illikainen, J. Yliniemi, Influence of ligands as chemical admixtures in the early hydration of sodium carbonate-activated blast furnace slag, Constr. Build. Mater. 422 (2) (2024), https://doi.org/10.1016/j. conbuildmat.2024.135753. February.
- [8] T. Jiang, Y. Jin, H. Ye, Correlating slag chemistry to setting and mechanical behaviors of alkali-activated slag, Constr. Build. Mater. 338 (2) (2022), https://doi. org/10.1016/j.conbuildmat.2022.127661. February.
- [9] A. Adesina, Resources, Environment and Sustainability Performance and sustainability overview of sodium carbonate activated slag materials cured at ambient temperature, Resour. Environ. Sustain. 3 (2) (2021), https://doi.org/ 10.1016/j.resenv.2021.100016. February.
- [10] A. Blotevogel, Simon Ehrenberg, L. Steger, L. Doussang, J. Kaknics, C. Patapy, M. Cyr, Ability of the R3 test to evaluate differences in early age reactivity of 16 industrial ground granulated blast furnace slags (GGBS), Cem. Concr. Res. 130 (2) (February, 2020), https://doi.org/10.1016/j.cemconres.2020.105998.

- [11] M. Ben Haha, B. Lothenbach, G. Le Saout, F. Winnefeld, Influence of slag chemistry on the hydration of alkali-activated blast-furnace slag — Part II: effect of Al₂O₃, Cem. Concr. Res. 42 (1) (2012) 74–83, https://doi.org/10.1016/j. cemconres.2011.08.005.
- [12] X. Dai, Q. Ren, S. Aydin, M.Y. Yardimci, G. De Schutter, Accelerating the reaction process of sodium carbonate-activated slag mixtures with the incorporation of a small addition of sodium hydroxide/sodium silicate, Cem. Concr. Compos. 141 (January) (2023) 105118, https://doi.org/10.1016/j.cemconcomp.2023.105118.
- [13] S.A. Bernal, J.L. Provis, R.J. Myers, R. San Nicolas, J.S.J. van Deventer, Role of carbonates in the chemical evolution of sodium carbonate-activated slag binders, Mater. Struct. Constr. 48 (3) (2014) 517–529, https://doi.org/10.1617/s11527-014-0412-6.
- [14] X. Liu, P. Feng, Y. Cai, X. Yu, C. Yu, Q. Ran, Carbonation behavior of calcium silicate hydrate (C-S-H): its potential for CO2 capture, Chem. Eng. J. 431 (P3) (2022) 134243, https://doi.org/10.1016/j.cej.2021.134243.
- [15] A. Aziz, et al., Enhancing sustainability in self-compacting concrete by optimizing blended supplementary cementitious materials, in: Scientific Reports, Nature Publishing Group UK, 2024, pp. 1–23, https://doi.org/10.1038/s41598-024-62499-w.
- [16] T. Luukkonen, Z. Abdollahnejad, K. Ohenoja, P. Kinnunen, Suitability of commercial superplasticizers for one- part alkali-activated blast-furnace slag mortar, J. Sustain. Cem. Mater. 4 (6) (2019) 1–14, https://doi.org/10.1080/ 21650373.2019.1625827. June.
- [17] Z. Xu, et al., Research on cement hydration and hardening with different alkanolamines, Constr. Build. Mater. 141 (2017) 296–306, https://doi.org/ 10.1016/j.conbuildmat.2017.03.010.
- [18] L. Chi, W. Li, Z. Li, Z. Wang, S. Lu, Q. Liu, Investigation of the hydration properties of cement with EDTA by alternative current impedance spectroscopy, Cem. Concr. Compos. 126 (8) (2022) 1–11, https://doi.org/10.1016/j. cemconcomp.2021.104365. August.
- [19] P.J.L. Ghorbani, Saeid Stefanini, Laura Sun Yubo, B. Walkley, J.L. Provis, G. De Schutter, S. Matthys, Characterisation of alkali-activated stainless steel slag and blast-furnace slag cements, Cem. Concr. Compos. 143 (6) (2023), https://doi.org/10.1016/j.cem.concomp.2023.105230. June.
- [20] S. Bagheri, O. Mankinen, S. Ojala, V. Telkki, T. Luukkonen, J. Yliniemi, 3, 4-dihydroxybenzoic acid forms soluble complexes in cementitious systems, J. Non-Cryst. Solids 633 (11) (2024), https://doi.org/10.1016/j.jnoncrysol.2024.122962. November.
- [21] K.A. Snyder, X. Feng, B.D. Keen, T.O. Mason, Estimating the electrical conductivity of cement paste pore solutions from OH, K⁺ and Na⁺ concentrations, Cem. Concr. Res. 33 (6) (2003) 793–798, https://doi.org/10.1016/S0008-8846(02)01068-2.
- [22] Y. Li, C.S.Q. Ding, Study on the cracking process of cement-based materials by AC impedance method and ultrasonic method, J. Nondestruct. Eval. 285 (9) (2012) 284–291, https://doi.org/10.1007/s10921-012-0142-z. June.
- [23] M. Ortega, Impedance spectroscopy study of the effect of environmental conditions on the microstructure development of sustainable fly ash cement mortars, Materials 10 (25) (2017). https://doi.org/10.3390/ma10101130. September.
- [24] M. Based, D.B. Istuque, A. Ot, M. Bortoletto, Impedance spectroscopy as a methodology to evaluate the reactivity of activated binder, Materials 15 (25) (November, 2022), https://doi.org/10.3390/ma15238387.
- [25] R.G. Torrents, J. Roncero, Utilization of impedance spectroscopy for studying the retarding effect of a superplasticizer on the setting of cement, Cem. Concr. Res. 28 (9) (1998) 1325–1333, doi: pii s0008-8846(98)00110-0.
- [26] Z. Xu, P. Gu, P. Xie, J.J. Beaudoin, Application of A.C. impedance techniques in studies of porous cementitious materials (III): ACIS behavior of very low porosity cementitious systems, Cem. Concr. Res. 23 (5) (1993) 1007–1015, https://doi.org/ 10.1016/0008-8846(93)90166-B.
- [27] A.K.H. Kwan, W.W.S. Fung, H.H.C. Wong, Water film thickness, flowability and rheology of cement-sand mortar, Adv. Cem. Res. 22 (1) (2010) 3–14, https://doi. org/10.1680/adcr.2008.22.1.3. March.
- [28] L. Chi, Z. Wang, S. Lu, D. Zhao, Y. Yao, Development of mathematical models for predicting the compressive strength and hydration process using the EIS impedance of cementitious materials, Constr. Build. Mater. 208 (11) (2019) 659–668, https://doi.org/10.1016/j.conbuildmat.2019.03.056. March.
- [29] L. Chi, T. Du, S. Lu, W. Li, M. Wang, Electrochemical impedance spectroscopy monitoring of hydration behaviors of cement with Na₂CO₃ accelerator, Constr.

- Build. Mater. 357 (6) (2022) 1–14, https://doi.org/10.1016/j.conbuildmat.2022.129374. June.
- [30] Emerson process Management, Conductance Data for Commonly Used Chemicals, 2010, 44-6039/rev.B.
- [31] N. Matthes, Winnie, Vollpracht Anya Villagrán, Yury Kamali-Bernard, Siham Hooton, Doug Gruyaert, Elke Soutsos, Marios De Belie, Ground granulated blast-furnace slag, in: Properties of Fresh and Hardened Concrete Containing Supplementary Cementitious Materials, vol. 25, RILEM State-of-the-Art Reports, 2018, pp. 1–53, https://doi.org/10.1007/978-3-319-70606-1_1.
- [32] O.H. Hussein, J. Provis, Effect of testing condition on the loss on ignition results of anhydrous granulated blast furnace slags determined via thermogravimetry Transformation of excavated London Clay into construction resources View project, in: International RILEM Conference on Materials, Systems and Structures in Civil Engineering Conference Segment on Concrete with Supplementary Cementitious Materials, Technical University of Denmark, Lyngby, Denmark, 2016, pp. 299–307 [Online]. Available: https://www.researchgate.net/publication/ 316969027.
- [33] K. Scrivener, R. Snellings, B. Lothenbach, A Practical Guide to Microstructural Analysis of Cementitious Materials, Taylor & Francis Group, 2016, https://doi.org/ 10.1201/b19074
- [34] R. Tänzer, A. Buchwald, D. Stephan, Effect of slag chemistry on the hydration of alkali-activated blast-furnace slag, Mater. Struct. Constr. 48 (3) (2014) 629–641, https://doi.org/10.1617/s11527-014-0461-x.
- [35] A. Boudedja, A. Hannou, S.B.E.N. Abdesselam, M. Almansba, R. Ferhoum, M. Habak, Experimental studies of granulated blast furnace slag. https://doi. org/10.37904/metal.2020.3450, 2020.
- [36] B. Lothenbach, A. Gruskovnjak, Hydration of alkali-activated slag: thermodynamic modelling, Adv. Cem. Res. 19 (1) (2014) 81–92, https://doi.org/10.1680/ adcr.2007.19.2.81. January.
- [37] Metrohm, "User manual for NOVA software [Online]. Available:, version 2.1.5, 2021. https://www.metrohm.com/fi fi/service/software-center/nova.html.
- [38] P. Liu, Lang Yang, B. Zhang, C. Huan, L. Guo, Q. Yang, K. Song, Study on hydration reaction and structure evolution of cemented paste backfill in early-age based on resistivity and hydration heat, Constr. Build. Mater. 272 (17) (2021) 1–11, https:// doi.org/10.1016/j.conbuildmat.2020.121827. December.
- [39] Y. Tu, D. Liu, L. Yuan, T. Wang, Early hydration process and kinetics of concrete based on resistivity measurement, J. Adv. Concr. Technol. 19 (3) (2021) 196–206, https://doi.org/10.3151/jact.19.196, March.
- [40] Z. Li, D. Lu, X. Gao, Analysis of correlation between hydration heat release and compressive strength for blended cement pastes, Constr. Build. Mater. 260 (31) (2020) 1–8, https://doi.org/10.1016/j.conbuildmat.2020.120436. August.
- [41] H. Uchikawa, S. Hanehara, D. Sawaki, The role of steric repulsive force in the dispersion of cement particles in fresh paste prepared with organic admixture, Cem. Concr. Res. 27 (1) (1997) 37–50, https://doi.org/10.1016/S0008-8846% 2896%2900207-4.
- [42] X. Hu, C. Shi, X. Liu, J. Zhang, G. De Schutter, A review on microstructural characterization of cement-based materials by AC impedance spectroscopy, Cem. Concr. Compos. 100 (August 2018) 1–14, https://doi.org/10.1016/j. cemconcomp.2019.03.018, 2019.
- [43] Q. L. F., F.P. Glasser, Microstructure, mass transport and densification of slag cement pastes, Mater. Res. Soc 16 (1) (2022) 1–23, https://doi.org/10.1557/proc-178-57
- [44] A.F. Sosa Gallardo, J.L. Provis, Electrochemical cell design and impedance spectroscopy of cement hydration, J. Mater. Sci. 56 (2) (2021) 1203–1220, https:// doi.org/10.1007/s10853-020-05397-6.
- [45] R.J. Flatt, Dispersion forces in cement suspensions, Cem. Concr. Res. 34 (19) (2004) 399–408, https://doi.org/10.1016/j.cemconres.2003.08.019. August.
- [46] E. Marzluff, PHYSICAL CHEMISTRY, California State University: LibreTexts libraries, 2024. https://chem.libretexts.org/@go/page/427300.
- [47] J. Sosa Gallardo, A.F., Provis, Early-age characterisation of Portland cement by impedance spectroscopy, Adv. Cem. Res. 34 (12) (2022) 542–559, https://doi.org/ 10.1680/jadcr.21.00103. December.
- [48] O. Bernard, J. Aupiais, Conductivity of weak electrolytes for buffer solutions: modeling within the mean spherical approximation, J. Mol. Liq. 272 (2018) 631–637, https://doi.org/10.1016/j.molliq.2018.09.103.